



---

MSc Thesis

---

# Identification and Simulation Study of Mixing Inrush Water Source Based on PHREEQC

---

Yixuan GAO

06/05/2019



---

School of Geoscience and Surveying Engineering  
China university of mining and technology, Beijing  
Beijing, Haidian district, Xueyuan road, ding 11  
Zonghe Building 619  
Phone: +86 17801156781  
[gyx1991728@163.com](mailto:gyx1991728@163.com)

---

## **Declaration of Authorship**

---

„I declare in lieu of oath that this thesis is entirely my own work except where otherwise indicated. The presence of quoted or paraphrased material has been clearly signaled and all sources have been referred. The thesis has not been submitted for a degree at any other institution and has not been published yet.”

---

## Abstract

---

Mine water inrush has become one of the common water hazards in the operation of mining enterprises. Once mine water inrush occurs, it will not only cause huge economic losses, but also threaten the lives of miners. The rapid and effective identification of the water inrush source is the basis for taking measures to control the water inrush when the mine water inrush accident occurs.

At present, the existing hydrogeochemical method is a powerful means to identify the source of mine water inrush. However, all kinds of methods need to be further studied, especially the advantages of computer technology in computing and simulation need to be fully utilized. In the mines of North China, there are few studies on the hydrochemical characteristics of mixed aquifers, especially on the hydrochemical types and the variation of ion concentration of mixed groundwater samples. Moreover, the current mine water inrush water source discrimination model is mostly established for a single water source. There are few studies on the discriminant model of mixed water inrush source, especially few studies on the discriminant model of mixed water inrush source based on artificial neural network technology.

Therefore, taking Jinggezhuang Mine in Kailuan Mining Area as the object of analysis, this paper collected and collated the water quality data obtained from many years' observation in the mining area. Mixing simulation of water sample data was carried out by PHREEQC hydrochemical simulation software, and its hydrochemical characteristics were analyzed. The establishment method of identification mixed inrush water source in mining area is studied. The following conclusions are drawn:

(1) The water quality types of aquifers in Kailuan Jinggezhuang mining area are analyzed by Piper Diagram. The hydrochemical characteristics of groundwater in Jinggezhuang Mine are generally characterized by high concentration of  $\text{Ca}^{2+}$ ,  $\text{K}^{+}+\text{Na}^{+}$ ,  $\text{HCO}_3^{-}$ . The hydrochemical types of Ordovician limestone karst fissure confined aquifer (I) and sand-gravel pore aquifer in upper Quaternary (VIII) are mainly  $\text{HCO}_3\text{-Ca}$  type, and those of sandstone fissure aquifer above coal 5 (V) are mainly  $\text{HCO}_3\text{-Na}$  type.

(2) The mix of groundwater samples were simulated hydrochemically by PHREEQC software in Jinggezhuang mining area. The hydrochemical types of mixed water

samples changed between  $\text{HCO}_3\text{-Ca}$  and  $\text{HCO}_3\text{-Na}$ , and the ion concentration also changed greatly. The main ions that changed were  $\text{Ca}^{2+}$ ,  $\text{K}^+\text{+Na}^+$ ,  $\text{HCO}_3^-$ , which were anions and cations with higher ion concentration in water samples.

(3) A TensorFlow-based artificial neural network mixed water source identification model is proposed. After data pre-processing and data standardization, cross-entropy error loss function and excitation function are used to reduce errors. Then, ADAM Optimizer is used to optimize the identification model. Finally, the data of water samples are trained and tested iteratively for several times to ensure that training accuracy of the neural network identification model is almost 90%, and that the identification accuracy of the neural network identification model for mixed water inrush sources reaches more than 80%.

Key words:

Hydrochemical characteristics analysis; groundwater mixing simulation; water inrush source identification; Kailuan mining area

---

## Table of Contents

---

Declaration of Authorship .....	II
Abstract .....	III
Table of Contents .....	V
1 Introduction .....	1
1.1 Research Background and Significance.....	1
1.2 Current Research Status.....	2
1.2.1 Study on Water Source Identification by Conventional Hydrochemistry.....	2
1.2.2 Study on Water Sources Identification by Isotopes and Trace Elements ....	5
1.3 Deficiencies of current research.....	6
1.4 Research Content and Research Methods .....	7
2 General Situation of Hydrogeology in Study Mining Area .....	9
2.1 Geological Situation of Kailuan Mining Area .....	9
2.2 Hydrogeological Conditions in Kailuan Mining Area.....	10
2.2.1 Characteristics of Regional Aquifers .....	10
2.2.2 Regional Hydrogeological Zoning.....	12
2.2.3 Recharge, Runoff and Discharge of Regional Karst Groundwater .....	13
3 Hydraulic-chemical Mixing Characteristic Analysis Based on PHREEQC. 15	
3.1 Introduction and Simulation Principle of PHREEQC.....	15
3.1.1 Introduction of PHREEQC.....	15
3.1.2 Simulating Principle of PHREEQC-Law of Mass Action .....	16
3.1.3 Simulating Principle of PHREEQC- Reaction Kinetics .....	17
3.2 Sampling and Data Acquisition.....	20
3.2.1 Groundwater Hydrochemical Data .....	20
3.2.2 Sampling and Testing.....	22
3.3 Hydrochemical Simulation by PHREEQC .....	22
3.3.1 Selection of Mixed Water Samples.....	23
3.3.2 Hydraulic-chemical Mixing Simulation by PHREEQC.....	25
3.4 Hydrochemical Characteristics Analysis of Mixing Simulation.....	27
3.4.1 Hydrochemical Characteristics of Water Samples.....	27
3.4.2 Hydrochemical Characteristics of Mixed Simulated Water Samples .....	30
4 Research on Identification Model of Inrush Water Source .....	37
4.1 Basic Ideas of BP Neural Network .....	37

4.2	Establishment of BP Neural Network Model for Recognition of Water Inrush Source.....	40
4.2.1	Data Preprocessing Method.....	41
4.2.2	Error Loss Function.....	41
4.2.3	Model Optimization by Gradient Descent Method.....	44
4.3	Verification of Water Inrush Source Identification in Jinggezhuang Mine..	47
4.4	Error Analysis.....	52
5	Conclusions and Innovation.....	54
5.1	Main Research Conclusions.....	54
5.2	Innovations.....	54
6	Bibliography.....	56
7	List of Figures.....	60
8	List of Tables.....	61

---

# 1 Introduction

---

This thesis studies unsafe acts of coal mine rescue accident, as well as their causes and the relationship between them.

This thesis collects and collates the water quality and hydrochemistry data obtained from many years 'observation in Kailuan mining area, simulates to mix the water samples by PHREEQC (a hydrochemistry simulation software), analyses their hydro-chemical characteristics, and studies the method of establishing the mixed proportion discrimination model of mine water inrush source.

---

## 1.1 Research Background and Significance

---

In the era of rapid development of coal industry, mining enterprises continue to increase mining intensity. The mining process makes the hydraulic connection between mine aquifers more complex. Various types of mine accidents occur from time to time, among which water accidents are particularly prominent (Qi R, 2018) .

Water inrush is one of the main disasters that endanger coal mine production. It not only causes direct economic losses and seriously restricts the production efficiency of coal mines, but also threatens the safety of mine geologists (Zhang D, 2017).

With the increase of mining demand, the mining depth of Kailuan mining area is increasing. The increase rate is about 8-12 m per year. Most of the mining areas in Kailuan are expected to reach a mining depth of 1000m in the future. Experiences at home and abroad, including Kailuan mining area, show that with the increase of mining depth, the in-situ stress, temperature and groundwater osmotic pressure increase correspondingly, the mining cost rises, and the underground working environment deteriorates. All these lead to the possibility of mine water inrush and other disasters greatly increased (Yang Z, 2011).

When the mine water inrush accident occurs, the primary task is to identify the source of water inrush quickly and accurately and provide direction for the follow-up disaster control work. Different water-filling sources have different water-filling intensity, and the corresponding treatment methods are also different. Therefore, only by quickly and accurately determining the source of water inrush, can we take effective measures to

control water inrush. In the mine water inrush disaster, there are not only single water inrush source, but also mixed water inrush sources. The research on the hydrochemical characteristics of mixing mine groundwater and the method of establishing the discriminant model for the mixed water source of inrush water can not only gain valuable time for effective measures to control inrush water disaster, but also provide a scientific theoretical basis for more precise and effective selection of water control measures (Jin Z, 2016).

Therefore, it is of great significance to study the mine groundwater mixing simulation and the identification of the mine water inrush multi-source, and to establish a scientific and effective identification model of the water inrush multi-source combining with the artificial neural network technology, so as to recognize the mining water inrush source timely and accurately after the occurrence of the water inrush and to prevent and control the water disaster.

---

## **1.2 Current Research Status**

---

At present, the commonly used technology to distinguish mine water inrush source is to obtain and analyze the hydrogeochemical information contained in groundwater, and distinguish the water inrush source according to hydrogeochemical information contained in the water quality. Combined with the groundwater level and water temperature in different aquifers, the source of water inrush can be distinguished from the hydrochemical, water temperature and hydrodynamic information of water inrush. The most simple, rapid and common method is hydrochemical analysis, which is based on the parameters of conventional hydrochemical characteristics, isotopes and trace elements. Hydrogeochemical analysis technology has many advantages in recognizing the source of mine water inrush, such as rapidity, timeliness, economy and convenience (Liu F, 2007).

---

### **1.2.1 Study on Water Source Identification by Conventional Hydrochemistry**

---

Conventional hydrochemical indexes include six major ions, hardness, alkalinity, temperature and pH value. Conventional hydrochemistry has some advantages, such as simplicity and rapidity of test method, familiarity with the site situation of Engineering technicians, so the research and application in this field is the most extensive and in-



depth. Conventional hydrochemical discriminant methods include traditional hydrochemical analysis method and uncertain mathematical statistics method.

In traditional hydrochemical methods, some analyze groundwater by directly describing the indicators, such as graphic method: Piper three-line diagram (based on the relative content of six major ions in water), Durov diagram, Langelier-Ludwig diagram, and one-component range method and two-component mapping method (Montety et al., 2010; O'Shea & Jankowski, 2010; Zhang X, Zhang Z & Peng S, 2003).

A large number of scholars have studied this method and applied it to identify the source of mine water inrush. Gui Herong (Gui H, Xu G & Song X, 2003) studied the relationship of concentration between  $\text{SO}_4^{2-}$  and  $\text{Cl}^-$  in groundwater, drew its Piper three-line map, analyzed and identified the water-filling conditions and water-filling sources of Taoyuan Coal Mine. Yang Jian (Yang J, Wang X, Li S, & Gao J, 2005) used Piper three-line graph analysis and mathematical statistical analysis to determine the difference of hydrochemical characteristics of each aquifer. The hydrogeochemical characteristics of Ordovician limestone aquifer, Taiyuan limestone aquifer, Shanxi sandstone fissure aquifer, Quaternary aquifer and coal aquifer in the groundwater system of a mine in Xuzhou were analyzed by conventional hydrochemical analysis method, which provided hydrogeochemical data source for the identification of mine water inrush source (Ge Z, Shen W & Bei H, 1994). The water inrush source of Xinhe Mine in Xuzhou City is identified based on the hydrochemical characteristics of each aquifer and the ratio of ion concentration in the aquifer, and the result is more accurate (Liu X, 1999). Yang Benshui (Yang B, Wang C & Yan C, 2003) analyzed the causes of water inrush in Qidong Coal Mine from four aspects: water level, water temperature, water quantity and water quality, and the results showed that the idea was feasible.

A great deal of successful experience has been gained in the research of identifying the source of water inrush by traditional hydrochemical methods. However, it is difficult to improve the accuracy of identification when the source of water inrush is not single, the type of water quality is complex and the chemical characteristics of water inrush are similar. In recent years, the combination of computer technology and the introduction of some uncertain mathematical and statistical methods have brought new ideas to the identification of water inrush sources, such as grey relational degree evaluation method, fuzzy mathematics comprehensive evaluation method, artificial neural network identification technology, multivariate statistical method, etc. The research of these

Identification and Simulation Study of Mixing Inrush Water Source

methods makes the identification methods of water inrush sources diversified, and the efficiency and accuracy of the identification have been significantly improved. The common idea is to rank the similarity between the chemical information data of water inrush samples and possible water sources, or the probability of water inrush. The maximum final result is determined as the source of water inrush.

Many scholars have made achievements in the research and application of grey relational degree evaluation method. Li Dongchen (Li D, 1995) used grey correlation analysis to identify the main aquifers in Baimiao Coal Mine, and used it in the determination of water inrush source. By studying the relationship between water inrush volume and water level change in each aquifer, the Grey Relational Degree Method is used to analyze and discriminate the super-large water inrush disaster in No. 2 617 working face of Yangzhuang Mine. Finally, the source of water inrush can be identified accurately (Zhou L & Li X, 1995). Gao Weidong et al. (Gao W, He Y & Li X, 2001; Sun Z & Gao W, 1995) analyzed the water inrush of Dongzhuang Coal Mine in Xuzhou Mining Area. The grey system theory is used to analyze the hydrochemical characteristics of mine aquifer, and then a water source discrimination model is established.

In the application of comprehensive evaluation technology of fuzzy mathematics, Fan Jingzhou (Fan J, Li H, Xie F, & Pan G, 2000), Li Mingshan (Li M, 1995; Li M et al., 2001), and Xia Xiaohong (Xia X, Zhang H & Yang W, 2002) established a discriminant model of Mine Water Inrush Source Based on the theory of fuzzy mathematics by utilizing the test data of water samples retained in the mine production process. The results show that the effect of the comprehensive discriminant technology of fuzzy mathematics is credible.

Artificial neural network technology also plays an important role in water source identification. When establishing discriminant model, lithology, structure, water pressure, aquifer thickness and aquifer thickness are taken into account. At the same time, the comprehensive effects of isotope, salinity, pH and other factors are considered. The training and testing of water samples show that the combination of computer technology and hydrogeology has a high reliability (Jiang C & Zhang S, 2006; Lei X, Zhang J & Xie T, 2003; Li D, 1998; Wei Y, Liang H, Ren Y & Liu W, 2004). Multivariate statistical analysis is also a very effective method for water source identification. The common method is multi-class stepwise linear discriminant based on Bayesian criterion.

Identification and Simulation Study of Mixing Inrush Water Source

The judgement results were tested by F distribution. This method has great advantages in the determination of unknown water samples. It has been applied in Renlou Mine in North Anhui Province and Jiaozuo Mine in Henan Province, proving that the actual effect is very good (Chen C et al., 1996; Song X, Gui H & Chen L, 2005; Sun B, Duan Z & Jin H, 1999; Zhang Y & Jiang Z, 2003).

---

### **1.2.2 Study on Water Sources Identification by Isotopes and Trace Elements**

---

Although the attempts of conventional hydrochemical discrimination provide a new way to distinguish the source of water inrush, the construction of the technology still depends on finding the "typomorphic" components of different aquifers. For some aquifers with similar water quality, this is often difficult. Although the contents of "trace elements" and "isotopes" in hydrochemical components are very small, they contain rich and unique hydrogeochemical information. Therefore, the characteristic information can be used to distinguish water sources. Combining with conventional components will achieve better discriminant effect (Bhat & Jeelani, 2015; Clark & Fritz, 1997; Davis & Ashenberg, 1989; Epstein & Mayeda, 1953; Gammons et al., 2006; Meng & Liu, 2016).

The most mature technologies used in the application of isotope technology are  $^{18}\text{O}$ , D and T.  $^{18}\text{O}$  and D are stable isotopes with tracer function, so as to find out the cause of formation of regional groundwater and the relationship between recharge and drainage. T is a radioisotope with the function of dating. It can be used to determine the age of groundwater to reflect the strength of regional water cycle. The stable isotope in groundwater reflects the fractionation of atmospheric components before the precipitation enters the underground, and its content will not change with time after entering the groundwater. This can be used to infer the origin of groundwater, the mixing effect and degree of various water bodies. Therefore, many scholars have applied environmental isotopes to identify the source of mine water inrush, and have achieved many research results. Cheng Chunqi et al. (Cheng C, Ge X & Wang D, 1994) analyzed the environmental isotope composition characteristics of aquifer in Baishan mining area and found out the typomorphic components as natural tracers to identify the source of mine water inrush. Gui Herong and Chen Luwang (Chen L et al, 2003; Gui H, Chen L & Song X, 2004; Gui H & Chen L, 2005) discussed the origin, recharge, runoff and drainage relationship of groundwater and the hydraulic relationship between aquifers based on  $^{18}\text{O}$ , D and T environmental isotope test data in Wanbei mining area,

and established the isotope water source discrimination model, which provided a new method for water source identification. Wang Guangcai et al. (Wang G, Duan Q, Bu C, & Chen S, 2001) further validated and corrected the conceptual model of water flow system in Pingdingshan mining area by using environmental isotope (hydrogen and oxygen) technology.

In the prevention and control of water inrush disaster in coal mine, the technology of water source identification based on trace elements is in its infancy. There are not many mining areas where this technology has been applied in practice (Chen L, Gui H, 2007). Song X, Gui H and others (Song X, Gui H & Chen L, 2004) established Bayes multi-class linear discriminant model of trace elements based on the analysis of conventional ions and trace elements in main aquifer water in the study of water inrush source discrimination in Huaibei Coalfield. Chen Luwang et al. (Chen L, 2003; Gui H, Chen L & Peng Z, 2004) collected data of groundwater samples from deep aquifers, including 20 trace elements such as Ag, Al, As and Ba. The principal component analysis model of mining area in northern Anhui was established. The principal component analysis of trace elements in groundwater was carried out, and the groundwater composition was analyzed in depth.

Although trace elements and isotopes have many advantages in studying water flow field and identifying water source, their detection conditions are demanding and time-consuming. When water inrush occurs, it is necessary to distinguish the source of water quickly. In order to solve this contradiction, Guihe Rong and Chen Luwang studied the correlation between trace elements, isotopes and conventional hydrochemical components, in order to find out some conventional components to replace trace elements and isotopes. In this way, the discriminant effect is improved quickly. Trace elements and isotopes, due to their unique mechanism in hydrogeochemical processes, can make up for the weaknesses of conventional hydrochemical methods, which is an important research and development direction (Zhang R, 2008).

---

### **1.3 Deficiencies of current research**

---

The existing hydrogeochemical methods are powerful means to identify the source of mine water inrush, but the study of various methods needs to be further deepened. It is necessary to select specific and appropriate methods in all kinds of methods according to the specific problems of water source identification, or to improve and innovate the

existing methods. In addition, the future development of water source identification technology should make more use of the advantages of computer technology in calculation and simulation.

(1) At present, there are few studies on the hydrochemical characteristics of mixed aquifers, especially on the hydrochemical types and the variation characteristics of ion concentration of mixing groundwater. It is also rare to study the hydrochemical characteristics of mixing aquifers in Kailuan mining area of North China.

(2) At present, the identification model of mine water inrush source is mostly established for a single water source. The research on the discriminant model of mixed water inrush source is relatively few. Moreover, in the study of the discriminant model of mixed water sources, the artificial neural network technology is seldom used to discriminate.

---

## **1.4 Research Content and Research Methods**

---

This paper combines the comprehensive identification technology of outburst water source in the National Key Research and Development Program "Rapid Identification Technology and Equipment for Mine Water Inrush Source". Taking Jinggezhuang Mine in Kailuan Mining Area as the research area, based on the analysis of the hydrogeochemical characteristics of the main aquifers, the underground aquifers mixing process were simulated by PHREEQC hydrochemical simulation software. The discriminant model of mixed water inrush source is established.

Based on the above ideas, the research contents of this paper are as follows:

(1) Analysis of hydrochemical characteristics of Jinggezhuang mine.

The related data of Jinggezhuang Mine in Kailuan Mining Area were investigated, collected and sorted out. This paper will analyze the regional geological structure characteristics and hydrogeological conditions of Kailuan mining area, especially the lithology of the aquifer and the occurrence law of groundwater in the mining area. The aquifer of Jinggezhuang Mine in Kailuan Mining Area will be sampled. The concentration of conventional anions and cations in water samples will be determined by experiments and analyzed, which is the basis of data acquisition for the follow-up study.

(3) Hydraulic chemical mixing simulation based on PHREEQC.

According to the water chemical composition ( $\text{Na}^+$ 、 $\text{Ca}^{2+}$ 、 $\text{Mg}^{2+}$ 、 $\text{Fe}^{2+}$ 、 $\text{Fe}^{3+}$ 、 $\text{Al}^{3+}$ 、 $\text{NH}_4^+$ 、 $\text{Cl}^-$ 、 $\text{SO}_4^{2-}$ 、 $\text{CO}_3^{2-}$ 、 $\text{HCO}_3^-$ 、 $\text{NO}_3^-$ 、 $\text{NO}_2^-$ ) of the aquifers in the study area, the mixed simulation of different proportions of the aquifers in the Kailuan mining area was carried out based on the hydrochemical simulation software PHREEQC, Their hydrochemical characteristics were also analyzed.

#### (4) Discrimination model of mixed water source based on TensorFlow.

TensorFlow software and artificial neural network technology are combined to explore the method of establishing mixed discriminant model for mixed water sources. The accuracy of the model is tested by using the mixed simulated water sample data of Jinggezhuang mining area.

---

## **2 General Situation of Hydrogeology in Study Mining Area**

---

Kailuan mining area is located in Tangshan City, Hebei Province, with a mining history of 140 years. There are 11 mines in this area including Jinggezhuang Mine, Donghuantuo Mine, Fangezhuang Mine, Tangjiazhuang Mine, Zhaogezhuang Mine and Linxi Mine (Liu J, Chang J & Hun B, 2008).

---

### **2.1 Geological Situation of Kailuan Mining Area**

---

The strata of Kailuan coalfield belong to North China type deposits. The coal measures are Paleozoic Carboniferous-Permian coal-bearing formations. The coal measure basement is Cambrian-Ordovician strata. The upper overburden is Cenozoic Quaternary.

Kailuan coalfield belongs to concealed coalfield. It is a large NE-trending composite coal-bearing syncline structure. It belongs to grade IV tectonic unit in the geotectonic division. It is situated on the first-order tectonic unit-Sino-Korean quasi-platform and in the second-order tectonic unit-Yanshan subsidence zone. It is a compound coal-bearing Syncline in the caprock structure of the Yanshan cycle, which is Tangshan and Jixian depression folds (grade III tectonic units).

Kailuan coalfield includes four coal-bearing structures: Kaiping syncline, Cheshaoshan syncline, Jinggezhuang syncline and Xiguanyao syncline. The Kaiping syncline and Cheshaoshan syncline are both long-axis synclines with hidden anticlines in the middle of the Beiziyuan. These three constitute the framework of the coal field. Jinggezhuang syncline and Xigongyao syncline are secondary folds separated from the main syncline after the uplift of Fengshan-Chengzizhuang anticline on the northwest wing of Kaiping syncline.

Kaiping syncline is a large asymmetric syncline structure. The extension length is 60 km and the aspect ratio is about 5:1. The total area of syncline is about 800 km<sup>2</sup>. The axis is SE40 degree in the South and gradually turns to near EW direction to the east of Guye in the north. The strata in the northwest wing are steep and even inverted. The strata in the southeast wing are gentle, and a series of fold structures are developed. From north to south, there are folds including Dujunzhuang anticline, Lujiatuo anticline, Jinggezhuang syncline, Bigezhuang syncline, Nanyangzhuang anticline, Gaogezhuang syncline, Lixinzhuang syncline, Liu Tangbao anticline and Shengang syncline. Their

Identification and Simulation Study of Mixing Inrush Water Source

axes are obliquely intersected with the main syncline, forming a "side curtain" fold. The dip of strata is generally 10-15 degrees, rarely more than 30 degrees. There are also faulted structures in Kaiping syncline. The compressive and compressive-torsional thrust faults are mainly developed in the northwest wing of the syncline, while the tensional normal faults are predominant in the southeastern wing of the syncline.

---

## **2.2 Hydrogeological Conditions in Kailuan Mining Area**

---

Kailuan coalfield is adjacent to Yanshan in the north, and the elevation in hilly area is 50~400 m. There are ancient strata and sporadic coal measures strata exposed. The coalfield is located in the Alluvial-diluvial plain in front of the Yanshan Mountains with flat terrain and elevation of 3-70m. Kailuan coalfield is located in the southern margin of the middle section of Yanshan subsidence zone, which is an asymmetric syncline structure with steep north wing and gentle South wing.

The syncline basin lies in the low mountains to the north and in the plain to the south. Most of the syncline basins are hidden under the Quaternary alluvium. The surface water system in the area is not well developed. Shahe River distributed in the eastern part of the coalfield and Douhe river entering the coalfield from the western part are seasonal rivers, which mainly play the role of draining mine water. Water-rich characteristics of coal-bearing sandstone aquifers, mainly fissure aquifers depend on the degree of structural development. The Ordovician limestone aquifer in coal measure basement is well developed and water-rich. It poses a certain security threat to the mine in this area. The recharge of aquifers in the region is mainly atmospheric precipitation. At the same time, the existence of aquifer structure also provides conditions for overflow recharge between aquifers. The huge complex three-dimensional groundwater flow system in Kailuan mining area has multi-level characteristics. However, this multi-level structure is not only the result of topographic fluctuations, but also the deposition of heterogeneous strata.

---

### **2.2.1 Characteristics of Regional Aquifers**

---

Kailuan mining area has multi-layered pore and karst-fissure water-filled aquifers structure which are closely related to each other hydraulically. Generally, it can be divided into three main water-filled aquifer groups.

#### **(1) Coal aquifers**

Identification and Simulation Study of Mixing Inrush Water Source

Based on PHREEQC



The main water-filled aquifers in coal measures are medium-thick layered medium and fine sandstone fractured aquifers. Vertical fissures are well developed in these aquifers. Moreover, it has uniform distribution on the plane, close hydraulic connection and uniform confined head. Generally, it can be divided into 2 to 3 fractured aquifer formations with a thickness of 40 to 60m.

### (2) Water-filling aquifer of middle Ordovician super-thick carbonate rocks

The water-filled aquifer of the middle Ordovician carbonate rocks has a large sedimentary thickness, usually 200-800 M. Aquifer exposed area is larger and karst is more developed. Rainfall infiltration recharge intensity is higher. Large-scale group hole pumping tests show that the water-filled aquifer of the Ordovician super-thick carbonate rock is rich in water. Moreover, the hydraulic connection is good, and the water pressure transmission is fast. The formed landing funnel is flat and extends widely. Generally, a unified karst water seepage field can be formed in each hydrogeological unit. The water-filled aquifer of the middle Ordovician super-thick carbonate rock has the most obvious characteristics of heterogeneity and anisotropy. Hydraulic phenomena such as strip-like karst runoff zones and discontinuous flow in continuous media are strong evidences. Middle Ordovician carbonate aquifer, as the base confined aquifer of coal-bearing rock series, has a high water head pressure, which poses a great threat to the safe mining of overlying coal seams. The extent of this threat depends not only on the thickness, lithology and structure of the water-proof rock section from the coal seam to the Ordovician limestone roof interface, but also on the thickness of aluminous clay deposited on the undulating Middle Ordovician paleoweathering surface.

### (3) Quaternary unconsolidated porous water-filled aquifers

The Quaternary porous water-filled aquifers with a thickness of more than ten to several hundred meters is unconformably covered by coal measures and Ordovician lime aquifers, which is like a bridge connecting the hydraulic connection between them and forming a special "bridge" hydrogeological condition of the deposit. Therefore, whether thick clay aquiclude is deposited at the bottom of Quaternary is one of the key factors to determine the complexity of hydrogeological conditions of such deposits. If the clay aquifer at the bottom of Quaternary is deposited very thin at the concealed outcrop of the bedrock aquifer group and even completely absent in some areas, the loose pebble aquifer is directly deposited on the coal measures bedrock and Ordovician limestone karst aquifer.

Permeable or "overflow" supply conditions can be formed.

Identification and Simulation Study of Mixing Inrush Water Source

---

## 2.2.2 Regional Hydrogeological Zoning

---

Kailuan coalfield can be divided into two hydrogeological regions: Yanshan outcrop area (area I) and piedmont plain area (area II). It is further divided into six hydrogeological sub-areas.

Yanshan outcrop area (area I) includes four hydrogeological sub-areas: I<sub>1</sub> - gneiss fissure water area, I<sub>2</sub> - karst fissure diving area, I<sub>3</sub> - sandstone fissure water area and I<sub>4</sub> - Quaternary Intermountain diving area.

### (1) I<sub>1</sub> - gneiss fissure water area

The strata are Proterozoic gneiss and granitic gneiss. Structural weathering and denudation are strong, and fissures are well developed. The precipitation is recharged by direct infiltration and discharged in the form of falling springs with the discharge of 1-2 l/s. Spring water supplies alluvium in Piedmont valley, and its dynamics is controlled by precipitation.

### (2) I<sub>2</sub> - Karst fissure diving area

The lithology is the limestone of Great Wall System, Jixian System, Cambrian System and Ordovician System. The fracture rate is 0.9%-5.8%. The karst rate is generally 5%-50%. The water level of limestone near mountain area is generally controlled by topography and season. The depth of water level is 30-70m. The water-rich characteristics of this area is nonuniform. The water quality type is HCO<sub>3</sub>-Ca-Mg, and the salinity is less than 0.3 g/l.

### (3) I<sub>3</sub> - Sandstone Fractured Water Zone

Lithology is mainly Permian and Carboniferous sandstone. Fracture water seeps directly into the recharge area. The mine water inflow is 480~600 m<sup>3</sup>/h.

### (4) I<sub>4</sub> - Quaternary Intermountain diving area

Quaternary Intermountain diving areas are distributed in Intermountain basins, and the thickness of Quaternary is tens of meters. Among them, the sandy gravel and pebble layers are rich in water. The depth of water level is generally less than 5 m. The

recharge includes precipitation infiltration recharge and mountain spring recharge. The water quality belongs to  $\text{HCO}_3\text{-Ca-Mg}$  type with salinity less than 0.5g/l.

The piedmont plain area (area II) includes the Permian, Carboniferous sandstone fissure water area ( $\text{II}_1$ ) and the karst coverage area of the Piedmont plain ( $\text{II}_2$ ).

(1)  $\text{II}_1$  - Fractured water area of Permian and Carboniferous sandstone in Piedmont Plain

This area is located between the outcrop area of Kaiping syncline coal measures and the Ordovician limestone top boundary. The Cenozoic gravel and pebble aquifers cover the outcrop of Permian Carboniferous strata. Therefore, the hydraulic characteristics of sandstone aquifer are controlled by covered Cenozoic gravel, pebble aquifer water and underlying Ordovician limestone water. The latter two are the main recharge sources of coal aquifers. Water quality type is  $\text{HCO}_3\text{-Ca-Mg}$ . Salinity is less than 0.3g/l. The maximum mine water inflow is 1860 ~ 2400  $\text{m}^3/\text{h}$ .

(2)  $\text{II}_2$  - karst coverage area of Piedmont Plain

The area is situated on the outer side of Kaiping syncline coal measure strata. It is a direct contact zone between Cenozoic alluvium and Ordovician limestone. The structure of the bedrock in this area is complex, and the thickness of the Cenozoic Alluvial-diluvial layer is very large. Among them, the aquifer properties of gravel and pebble layers are strong. The water inflow is more than 1 L/s·m, and the maximum is 22 L/s.m. Ordovician limestone karst fissures are well developed with strong water content. The water inflow is more than 1 l/s·m. There is no stable aquiclude between the two aquifers. There are close hydraulic connection between them. The water level and quality are basically the same. The water quality is  $\text{HCO}_3\text{-Ca-Mg}$  type and the salinity is 0.1-0.3 g/l. Groundwater runs from northeast to southwest. This area is the most active area of groundwater in Kaiping coalfield.

---

### **2.2.3 Recharge, Runoff and Discharge of Regional Karst Groundwater**

---

The low mountain and hilly area in the northern part of this area is a large area of exposed bedrock with an area of 1028  $\text{km}^2$ . The Great Wall, Jixian, Cambrian and Ordovician limestones account for more than 90%. The limestone karst fissures are

well developed and easy to be infiltrated by atmospheric precipitation. It is the main recharge area for groundwater to receive precipitation infiltration in this area.

After recharge, part of the groundwater flows downstream to the valley in the form of falling springs. The other part runs downstream along karst fissures or structural fissures to recharge groundwater in plain areas. There is still a small amount of evaporation. The hydraulic gradient is steep in the north and gentle in the south.

Because of topography, geomorphology and geological structure, there are two watersheds in the flow direction of groundwater in this area, which is the eastern Shahe watershed and the western Douhe watershed. The general groundwater flow is from northeast to southwest. At the axis of Kaiping syncline, the groundwater flow is blocked and the movement is relatively slow.

---

## **3 Hydraulic-chemical Mixing Characteristic Analysis Based on PHREEQC**

---

In order to further study the hydrochemical characteristics of the mixed aquifers in Kailuan mining area, this chapter uses the geochemical simulation software PHREEQC to simulate the mixed groundwater samples in the study area. The change of hydrochemical characteristics of groundwater during mixing process is further discussed.

---

### **3.1 Introduction and Simulation Principle of PHREEQC**

---

#### **3.1.1 Introduction of PHREEQC**

---

PHREEQC is a software specially used for hydrogeochemical simulation. The computer program written in C language was developed by the Geological Survey Bureau of the United States. The predecessor of this software is Phreeqe, which improves the hydrochemical simulation function by continuously developing all functions compatible with Phreeqe and Netpath. Because of its powerful function, PHREEQC is often used in various hydrogeochemical simulation tasks, including forward and reverse path simulation, mixing simulation, evaporation and redox reaction. Therefore, it is applied to almost all equilibrium thermodynamics and chemical kinetics problems in the interaction system of water, gas and rock.

Water in underground aquifers is a solution of multiple solutes. Elements in solution can be described by a series of equations in PHREEQC, including water activity, ionic strength, charge balance of solution, mass balance of adsorbent surface, etc. During the simulation, the input commands are selected according to different equations describing the chemical reaction process.

PHREEQC hydrochemical simulation software includes four parts: input file, output file, selective output file and database. The input file is a text file that gives commands for model reading and simulation, and is written by users. The output file is the result file after the software operation. Selective output files can select output results according to user needs. The database file provides expressions for ionic mineral constants and soluble precipitation, redox, dynamic equilibrium chemical reactions, etc. (Zhang P, 2017).

Identification and Simulation Study of Mixing Inrush Water Source

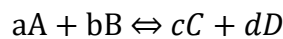
Based on PHREEQC

---

### 3.1.2 Simulating Principle of PHREEQC-Law of Mass Action

---

The law of mass action is the basis of hydrogeochemical simulation calculation. It means that the driving force of a chemical reaction is related to the concentration of the reactant and the concentration of the product. The hypothetical responses are as follows:



In the above formula, a is the number of moles of reactant A, b is the number of moles of reactant B, c is the number of moles of biological C and d is the number of moles of biological D. When the above reaction method reaches equilibrium, the following relationship exists:

$$\frac{[C]^c + [D]^d}{[A]^a + [B]^b} = K$$

In the formula:  $[\ ]$  represents the activity of the reactant or product, and K is the thermodynamic equilibrium constant. In the formula above, the left side of the equal sign is also called activity product. When all the components involve in the reaction are ions, it is called ion activity product, which will be expressed by IAP.

In non-ideal solution groundwater, activity is the corrected value of the measured concentration of various components, which can be expressed by the following expressions:

$$\alpha = \gamma \cdot c$$

In the formula,  $\alpha$  represents activity with no dimension. c is the measured concentration of the constituents participating in the chemical reaction in units of mole per liter.  $\gamma$  is the activity coefficient. In hydrogeochemical simulation studies, Bayer-Shocker equation is often used to calculate activity coefficient  $\gamma$ . The activity coefficients  $\gamma$  of groundwater are usually less than 1. The specific calculation equations are as follows:

$$\tan \gamma = \frac{-A \cdot Z^2 \cdot \sqrt{I}}{1 + Ba\sqrt{I}}$$

Ion strength I is calculated by the following formula:

$$I = \frac{1}{2} \sum Z_i^2 \cdot c_i$$

$c_i$  – The concentration of ion i in mmol/L;

$Z_i$  – Electric charge Number of ion i;

In order to understand the reaction state between minerals and groundwater aqueous solution in the process of water-rock interaction, the saturation index SI of minerals in aqueous solution should be calculated. The formula for calculating the saturation index SI is as follows:

$$SI = \log \frac{IAP}{K}$$

IAP is the product of anionic and cationic activities of minerals in water.

K is the thermodynamic equilibrium constant at a certain humidity. When the saturation index SI of a mineral in water is bigger than 0, the mineral is in a supersaturated state and then precipitates. When the saturation index  $SI = 0$ , the mineral is in equilibrium. When the saturation index SI is less than 0, the mineral is unsaturated and dissolves (Wang L, 2012).

---

### 3.1.3 Simulating Principle of PHREEQC- Reaction Kinetics

---

Most studies on chemical reactions are based on thermodynamic equilibrium. It is assumed that the reaction system is a stable closed system independent of time. But this assumption is flawed. The law of thermodynamics cannot answer the time required for a reaction to reach equilibrium. Therefore, when the simulated reaction is slow, reversible, irreversible or inhomogeneous, the reaction kinetics, the rate at which the chemical reaction proceeds or reaches equilibrium, should be taken into account at the same time.

#### (1) Reaction Kinetics of Different Chemical Processes

Different chemical reactions have different half-lives, which is like isotope decay. Half-life is the time spent when half of the reactants react to produce the reaction products. The half-life is recorded as  $t_{1/2}$  and the retention time of groundwater is recorded as  $t_R$ . When  $t_{1/2} < t_R$ , it can be considered that the system is in equilibrium state, which can be simulated by thermodynamic equilibrium. When  $t_{1/2} > t_R$ , the system is not in equilibrium, so the dynamic model must be considered. The stability constants of acid-base reaction and complexation are relatively low. Some of the reactions are completed in microseconds or milliseconds. It is also a very fast reaction to form nonspecific

adsorption of disordered surface films. Thermodynamic equilibrium models are needed to solve these fast reactions. The reaction rate of ion exchange is mainly related to the bonding mode and the type of exchanger. Exchange reactions occurring only at the edge of particles, such as kaolinite, are the fastest. Exchanges that need to enter the mineral layer, such as montmorillonite, or those that need to enter the tight matrix layer, such as illite, proceed relatively slowly. The dissolution and precipitation reactions vary according to the situation. Some take only a few hours, while others take thousands of years to complete. Some reactions take thousands of years before half of the reactants are converted. So there are great differences in this reaction. For redox reaction, if there is no catalyst, its half-life will be longer. In conclusion, the kinetic reaction model needs to be considered for these slow reactions (Merkel, 2005).

## (2) Calculation of reaction rate

The reaction rate is a decrease in the concentration of reactants or an increase in the concentration of reactants per unit time along the groundwater flow. Normally, the reaction rate of positive reaction, taking  $A+B \rightarrow C$  as an example, is not the same as that of reverse reaction  $C \rightarrow A+B$ . The reaction kinetics of the whole reaction is actually the sum of the positive reaction rate and the inverse reaction rate, as follows:

$$v^+ = k^+ \prod_i (X_i)^{n_i}$$

$$v^- = k^- \prod_i (X_i)^{n_i}$$

$$K_{eq} = \frac{k^+}{k^-} = \prod_i (X_i)^{n_i}_{eq}$$

$V^+$  is the rate of positive reaction.

$V^-$  is the velocity of the inverse reaction.

$K^+$  is the rate constant of positive reaction.

$K^-$  is the velocity constant of the inverse reaction.

$X$  is a reactant or a reaction product.

$n$  is the stoichiometric coefficient.

$K_{eq}$  is the equilibrium constant.



In general, the chemical reactions we study are not completed in one step, but through several consecutive steps. At this time, the reaction rate of the whole reaction is controlled by the slowest one-step chemical reaction.

### (3) Factors affecting the reaction rate

Firstly, the reaction rate is closely related to the concentration of reactants and products. According to the collision theory, when the concentration is high, the probability of collision between ions will be higher, so that the reactants will transform faster. But not all collisions can cause reactions. The precondition for the reaction is that the molecule must have a suitable position to overcome certain activation energy, which is the energy that must be overcome in the reaction. In addition to the concentration, there are many factors affecting the reaction rate, such as pH value, temperature, organic composition and content, catalysts and surface active substances. Langmuir (1997) gave activation energies for different chemical reactions. The activation energy range of physical adsorption is 2-6 kcal/mol. The activation energy of diffusion in dissolution is less than 5 kcal/mol. The activation energy of mineral dissolution and precipitation ranges from 8 to 36 kcal/mol, while the activation energy of ion exchange is more than 40 kcal/mol.

Plummer et al. (1978) obtained the rate equation of carbonate dissolution and precipitation:

$$R_{calcite} = K_1 \cdot \{H^+\} + K_2 \cdot \{CO_2\} + K_3 \cdot \{H_2O\} - K_4 \cdot \{Ca^{2+}\}\{HCO_3^-\}$$

$K_1$ ,  $K_2$  and  $K_3$  are constants in the formula, which are temperature dependent. They are used to describe positive reactions.

$$K_1 = 10^{0.198-444.0/T_K}, \quad K_2 = 10^{2084-2177.0/T_K}$$

When the temperature is less than or equal to 25°C,  $K_3 = 10^{-5.86-317.0/T_K}$

When the temperature is larger than 25°C,  $K_3 = 10^{-1.1-1737.0/T_K}$

$K_4$  is used to describe adverse reactions,  $K_4 = 1 - \left(\frac{IAP}{K_{calcite}}\right)^{\frac{2}{3}}$

IAP is the product of ionic activity and  $K_{calcite}$  is the solubility product of calcite (Wang L, 2012).

---

## 3.2 Sampling and Data Acquisition

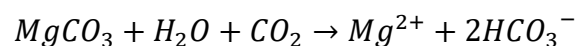
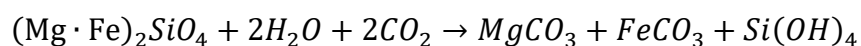
---

### 3.2.1 Groundwater Hydrochemical Data

---

Groundwater is a complex mixture containing many substances. In the lithosphere, groundwater is often closely related to rocks, influencing and reacting with each other. The water relationship between the earth's various spheres is complex, but there are certain rules to be found. There are also some differences in the chemical components and concentration relationship between their contents in different environments. Therefore, its chemical composition indicates the specific geological environment characteristics. The major hydrochemical data studied at home and abroad are groundwater constant ions, trace elements and isotopes. At present, there are six kinds of constant ions in groundwater chemical analysis,  $\text{Na}^+\text{K}^+$ ,  $\text{Ca}^{2+}$ ,  $\text{Mg}^{2+}$ ,  $\text{Cl}^-$ ,  $\text{SO}_4^{2-}$ ,  $\text{HCO}_3^-$ . Through the study and analysis of these conventional ions, the source of groundwater can be determined (Wu Y, 2018).

$\text{Ca}^{2+}$  is the main cation in low salinity groundwater. With the increase of salinity, the relative content of calcium ions decreases rapidly. This is due to the low solubility of calcium sulfate and calcium carbonate, resulting in the precipitation of gypsum and calcite.  $\text{Ca}^{2+}$  is derived from weathering and dissolution of carbonate sediments, gypsum sediments, magmatic rocks and metamorphic rocks containing calcareous minerals. The source and distribution of  $\text{Mg}^{2+}$  in groundwater are similar to that of calcium.  $\text{Mg}^{2+}$  comes from sediments containing magnesium carbonate (dolomite, marl), and weathering and dissolution of magnesium minerals in magmatic and metamorphic rocks (Yidana & Banoeng, 2010).

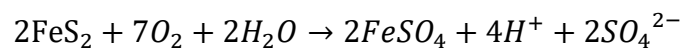


$\text{Na}^+$  is the main cation in high salinity water. It is a dissolved sodium salt, such as sedimentary rock salt, which can also be obtained from seawater. In magma and metamorphic areas, it is dissolved by weathering from sodium minerals. Acidic magma contains a large number of sodium-bearing minerals, such as albite. Therefore, with the participation of  $\text{CO}_2$  and  $\text{H}_2\text{O}$ , low mineralized groundwater with  $\text{Na}^+$  and  $\text{HCO}_3^-$  as the main ions will be formed.  $\text{K}^+$  comes from dissolved salts of potassium-bearing sediments and weathering and dissolution of potassium-bearing minerals in magmas

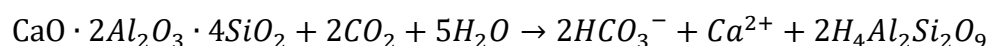
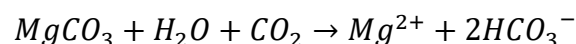
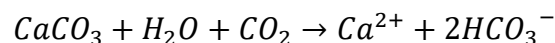
and metamorphic rocks. The source and distribution characteristics of  $K^+$  and  $Na^+$  in groundwater are similar, but the content of the former in groundwater is much less than that of the latter. This is because  $K^+$  is involved in the formation of secondary minerals (hydromica, montmorillonite and taenite) which are insoluble in water and are easily absorbed by plants. Generally, the two minerals are combined and analyzed (Li, Hui, Wu, Zhang, & Zhang, 2013).

$Cl^-$  is derived from the dissolution of rock salt or other chlorides in sedimentary rocks and weathering dissolution of chlorine-bearing minerals (chlorinated apatite  $Ca_5(PO_4)_3Cl$  and sodalite  $NaAlSi_3O_8 \cdot NaCl$ ) in magmatic rocks. Seawater also recharges groundwater. Sometimes wind from the sea brings frothy sea water to the land and leaching of volcanic eruptions, which also increases the content of  $Cl^-$  in groundwater. The content of  $Cl^-$  increases with the increase of salinity, which can be used to explain the degree of mineralization of groundwater (Yue et al., 2014).

$SO_4^{2-}$  comes from the dissolution of gypsum ( $CaSO_4 \cdot 2H_2O$ ) or other sulfate sedimentary rocks. Or the oxidation of sulfides causes S, which is formerly insoluble in water, to dissolve in large quantities in the form of  $SO_4^{2-}$  in water. Coal measures strata often contain a lot of pyrite, so the groundwater flowing through these strata often takes  $SO_4^{2-}$  as the main ion (WangBian & Gao, 2014).



$HCO_3^-$  is almost the main anionic component in low salinity water. It comes from carbonate-bearing sedimentary rocks and metamorphic rocks (such as marble). In the magmatic and metamorphic rock areas,  $HCO_3^-$  mainly comes from weathering and dissolution of aluminosilicate minerals (albite and calciferous feldspar).



In addition, the total salinity (or total dissolved solids, TDS) is often used as a conventional hydrochemical index.

---

### 3.2.2 Sampling and Testing

---

During many years of production, a large amount of hydrogeological data has been accumulated in Kailuan mining area. In order to study the hydrochemical characteristics of groundwater mixing, the data of aquifer water samples used in this project were collected at Xiaijinggezhuang Mine, Kailuan Mining Bureau, Tangshan City, Hebei Province. The water quality data of the water samples analyzed are mainly from the pebble pore confined aquifer at the bottom of Quaternary alluvium, the roof sandstone fissure aquifer of coal measure stratum 5, the 12 to 14 sandstone fissure aquifer of coal measure stratum, and the Ordovician limestone fissure confined aquifer of coal measure sedimentary basement.

The water samples collected in this study were used to determine their hydrochemical indicators. The test items mainly include pH,  $\text{Na}^+$  ( $\text{Na}^+\text{+K}^+$  is replaced by  $\text{Na}^+$  because of its low  $\text{K}^+$  content and similar chemical properties to  $\text{Na}^+$ ),  $\text{Ca}^{2+}$ ,  $\text{Mg}^{2+}$ ,  $\text{Cl}^-$ ,  $\text{SO}_4^{2-}$ ,  $\text{HCO}_3^-$ . The method of pH determination is glass electrode method,  $\text{HCO}_3^-$  test is acid-base indicator titration method,  $\text{Cl}^-$  and  $\text{SO}_4^{2-}$  test is ion chromatography method,  $\text{Ca}^{2+}$  and  $\text{Mg}^{2+}$  test is EDTA titration method,  $\text{Na}^+$  test is flame atomic absorption spectrophotometry.

---

### 3.3 Hydrochemical Simulation by PHREEQC

---

Mixing simulation can be realized by using PHREEQC hydrogeochemical simulation software. Mixing function can simulate the mixing of two water samples in different proportions, and ultimately get the water sample information in equilibrium state. Forward simulation can use the given composition of water samples and ion concentration to simulate the mixing equilibrium. The specific contents of ions in saturated water samples were calculated.

In the main aquifer water samples, four groups of water samples with representative characteristics are selected in each aquifer for two-to-two mixing, and the mixing ratio is from 1:9 to 9:1.

### 3.3.1 Selection of Mixed Water Samples

Taking Jinggezhuang Mine as an example, water samples from representative aquifers are selected for hydrochemical mixing simulation.

Ordovician limestone karst fissure confined aquifer (I), sandstone fissure aquifer above coal 5 (V) and sand-gravel pore aquifer in upper Quaternary (VIII) are selected as representative aquifers, and four representative water samples are selected for each aquifer.

The hydrochemical information and hydrochemical types of the selected aquifers are shown in Table 1 Hydrochemistry information of the Ordovician limestone aquifer water samples, Table 2 Hydrochemistry information of the sandstone fissure aquifer water samples, Table 3 Hydrochemistry information of the Quaternary alluvial aquifer water samples.

Hydrochemical indices	Water sample			
	O1	O2	O3	O4
pH	7.84	7.85	8.00	8.10
Na <sup>+</sup> (mg/L)	11.63	10.90	11.16	5.58
Ca <sup>2+</sup> (mg/L)	46.35	31.75	43.55	36.41
Mg <sup>2+</sup> (mg/L)	12.70	10.66	19.11	8.27
Fe <sup>2+</sup> (mg/L)	0.00	0.00	0.00	0.00
Fe <sup>3+</sup> (mg/L)	0.00	0.00	0.04	0.04
Al <sup>3+</sup> (mg/L)	0.00	0.03	0.37	3.01
NH <sup>+</sup> (mg/L)	0.00	0.00	0.00	0.00
Cl <sup>-</sup> (mg/L)	18.96	7.72	7.27	7.76
SO <sub>4</sub> <sup>2-</sup> (mg/L)	15.71	7.00	12.96	9.25
HCO <sup>-</sup> (mg/L)	153.30	133.40	209.95	154.18
NO <sub>3</sub> <sup>-</sup> (mg/L)	30.34	9.00	2.64	3.94
NO <sub>2</sub> <sup>-</sup> (mg/L)	0.00	0.00	0.01	0.03

**Table 1 Hydrochemistry information of the Ordovician limestone aquifer water samples**

Hydrochemical indices	Water sample			
	S1	S2	S3	S4
pH	8.00	8.30	8.30	8.40
Na <sup>+</sup> (mg/L)	77.81	88.66	72.54	79.12
Ca <sup>2+</sup> (mg/L)	26.59	34.28	31.24	15.17
Mg <sup>2+</sup> (mg/L)	12.77	6.08	9.85	13.22
Fe <sup>2+</sup> (mg/L)	0.00	0.00	0.00	0.00
Fe <sup>3+</sup> (mg/L)	0.04	0.04	0.04	0.06
Al <sup>3+</sup> (mg/L)	1.03	1.69	1.16	1.01
NH <sup>+</sup> (mg/L)	0.00	0.00	0.00	0.00
Cl <sup>-</sup> (mg/L)	19.40	17.94	16.00	17.96
SO <sub>4</sub> <sup>2-</sup> (mg/L)	10.89	15.00	10.48	9.87
HCO <sup>-</sup> (mg/L)	257.79	261.81	254.19	275.42
NO <sub>3</sub> <sup>-</sup> (mg/L)	0.26	0.53	0.26	0.18
NO <sub>2</sub> <sup>-</sup> (mg/L)	0.00	0.00	0.00	0.00

**Table 2 Hydrochemistry information of the sandstone fissure aquifer water samples**

Hydrochemical indices	Water sample			
	C1	C2	C3	C4
pH	7.80	7.90	8.00	8.00
Na <sup>+</sup> (mg/L)	28.98	26.97	61.69	47.75
Ca <sup>2+</sup> (mg/L)	42.66	41.41	52.23	44.71
Mg <sup>2+</sup> (mg/L)	16.05	20.35	12.45	9.83
Fe <sup>2+</sup> (mg/L)	0.00	0.00	0.00	0.00
Fe <sup>3+</sup> (mg/L)	0.04	0.04	0.04	0.08
Al <sup>3+</sup> (mg/L)	1.03	0.50	0.76	0.20
NH <sup>+</sup> (mg/L)	0.00	0.00	0.00	0.00
Cl <sup>-</sup> (mg/L)	12.90	7.76	18.43	22.77
SO <sub>4</sub> <sup>2-</sup> (mg/L)	22.64	15.90	22.01	9.97
HCO <sup>-</sup> (mg/L)	242.18	250.02	287.05	250.94
NO <sub>3</sub> <sup>-</sup> (mg/L)	0.88	0.88	0.69	1.63

NO <sub>2</sub> <sup>-</sup> (mg/L)	0.01	0.01	0.02	0.02
-------------------------------------	------	------	------	------

**Table 3 Hydrochemistry information of the Quaternary alluvial aquifer water samples**

### 3.3.2 Hydraulic-chemical Mixing Simulation by PHREEQC

When mixing water samples from different aquifers, all combinations of four representative water samples from each aquifer and four representative water samples from another aquifer are considered. The mixing ratios were 1:9, 2:8, 3:7, 4:6, 5:5, 6:4, 7:3, 8:2 and 9:1, respectively. The simulated mixing of water samples in the confined aquifer of the Ordovician limestone karst fissure confined aquifer (I), sandstone fissure aquifer above 5 coal (V) and sand-gravel pore aquifer in the upper Quaternary (VIII) is shown in Table 4 Mixed assemblages of representative water samples from each aquifer.

Aquifer	Samples	Mixing ratio	Aquifer	Samples	Mixing ratio	Aquifer	Samples	Mixing ratio
Ordovician limestone aquifer and sandstone fissure aquifer	O1:S1	1:9-9:1	Ordovician limestone aquifer and Quaternary alluvial aquifer	O1:C1	1:9-9:1	sandstone fissure aquifer and Quaternary alluvial aquifer	S1:C1	1:9-9:1
	O1:S2	1:9-9:1		O1:C2	1:9-9:1		S1:C2	1:9-9:1
	O1:S3	1:9-9:1		O1:C3	1:9-9:1		S1:C3	1:9-9:1
	O1:S4	1:9-9:1		O1:C4	1:9-9:1		S1:C4	1:9-9:1
	O2:S1	1:9-9:1		O2:C1	1:9-9:1		S2:C1	1:9-9:1
	O2:S2	1:9-9:1		O2:C2	1:9-9:1		S2:C2	1:9-9:1
	O2:S3	1:9-9:1		O2:C3	1:9-9:1		S2:C3	1:9-9:1
	O2:S4	1:9-9:1		O2:C4	1:9-9:1		S2:C4	1:9-9:1
	O3:S1	1:9-9:1		O3:C1	1:9-9:1		S3:C1	1:9-9:1
	O3:S2	1:9-9:1		O3:C2	1:9-9:1		S3:C2	1:9-9:1
	O3:S3	1:9-9:1		O3:C3	1:9-9:1		S3:C3	1:9-9:1
	O3:S4	1:9-9:1		O3:C4	1:9-9:1		S3:C4	1:9-9:1
	O4:S1	1:9-9:1		O4:C1	1:9-9:1		S4:C1	1:9-9:1

O4:S2	1:9- 9:1	O4:C2	1:9- 9:1	S4:C2	1:9- 9:1
O4:S3	1:9- 9:1	O4:C3	1:9- 9:1	S4:C3	1:9- 9:1
O4:S4	1:9- 9:1	O4:C4	1:9- 9:1	S4:C4	1:9- 9:1

**Table 4 Mixed assemblages of representative water samples from each aquifer**

With the mixing function MIX in PHREEQC, the hydrochemical information of the above water samples can be input and saved. The mixing ratio is set to 1:9, 2:8, 3:7, 4:6, 5:5, 6:4, 7:3, 8:2 and 9:1. The equilibrium term of the possible products is added and the mixed water sample is preserved. The chemical information that needs to be output such as constant ion weight and pH of each mixed solution are needed to select and set. Finally, save the file and click Run button to simulate to get and save the results. A total of 432 water samples were obtained after mixing.

**Because of the limited space, this paper takes mixing simulation of water sample O1 from Ordovician limestone karst fissure confined aquifer (I) and water sample C1 from sand-gravel pore aquifer in the upper Quaternary (VIII) as an example to illustrate. The mixing simulation results are processed and the severity is converted into concentration information. The mixing results are shown in the**

**Table 5 Mixing simulation results of water sample O1 and C1 in Jinggezhuang Mine..**

Mixing ratio	1:9	2:8	3:7	4:6	5:5	6:4	7:3	8:2	9:1
pH	7.51	7.52	7.53	7.54	7.55	7.56	7.57	7.59	7.60
Na <sup>+</sup> mg/L	27.27	25.53	23.79	22.06	20.32	18.58	16.85	15.11	13.37
Ca <sup>2+</sup> mg/L	38.02	38.70	39.38	40.06	40.74	41.41	42.08	42.74	43.39
Mg <sup>2+</sup> mg/L	15.52	15.19	14.86	14.53	14.20	13.87	13.54	13.21	12.88
Fe <sup>2+</sup> mg/L	0.00	0.00	0.00	0.00	0.00	0.00	0.00	0.00	0.00
Fe <sup>3+</sup> mg/L	0.03	0.03	0.03	0.02	0.02	0.02	0.01	0.01	0.00



Al <sup>3+</sup>	0.93	0.82	0.72	0.62	0.52	0.41	0.31	0.21	0.10
mg/L									
NH <sup>+</sup>	0.00	0.00	0.00	0.00	0.00	0.00	0.00	0.00	0.00
mg/L									
Cl <sup>-</sup>	13.53	14.14	14.74	15.35	15.96	16.56	17.17	17.78	18.38
mg/L									
SO <sub>4</sub> <sup>2-</sup>	21.95	21.25	20.56	19.87	19.17	18.48	17.79	17.09	16.40
mg/L									
HCO <sup>-</sup>	225.83	217.42	209.00	200.59	192.16	183.74	175.30	166.86	158.40
mg/L									
NO <sub>3</sub> <sup>-</sup>	3.83	6.78	9.72	12.67	15.61	18.55	21.50	24.44	27.39
mg/L									
NO <sub>2</sub> <sup>-</sup>	0.00	0.00	0.00	0.00	0.00	0.00	0.00	0.00	0.00
mg/L									

**Table 5 Mixing simulation results of water sample O1 and C1 in Jinggezhuang Mine.**

### 3.4 Hydrochemical Characteristics Analysis of Mixing Simulation

The hydrogeological conditions of Jinggezhuang Mine in Kailuan Mining Area are complex and the water-filling sources are diverse. The hydrochemical characteristics of different aquifers are different. After mixing, some changes have taken place in the hydrochemical characteristics of the aquifer samples, which are different from the original ones.

#### 3.4.1 Hydrochemical Characteristics of Water Samples

##### (1) Ordovician limestone karst fissure confined aquifer (I)

This aquifer is more than 600 m thick, mainly located in the southeastern part of the well field. The lithology of the aquifer is leopard skin limestone and dolomitic limestone. The development of limestone fissures is increased because of the contact between tectonism and quaternary alluvium. The water inflow of the aquifer ranges from 0.664 to 1.553 L/s·m, with an average of 1.108 L/s·m. The permeability coefficient is 2.3227 - 4.9458 m/d, with an average of 3.63425 m/d. The aquifer is rich in water.

According to drilling data, the borehole enters within 100 meters of Ordovician limestone. The above properties do not change significantly with depth. There are two aquifers between Ordovician limestone and 12-2 coal seam, namely K<sub>2</sub> - K<sub>6</sub> and K<sub>6</sub> - 12

coal-rock fissure aquifers, whose thickness is 100m and 20m respectively. The hydrochemical characteristics Piper three-line diagram of the representative water samples of this aquifer are shown in Figure 1.

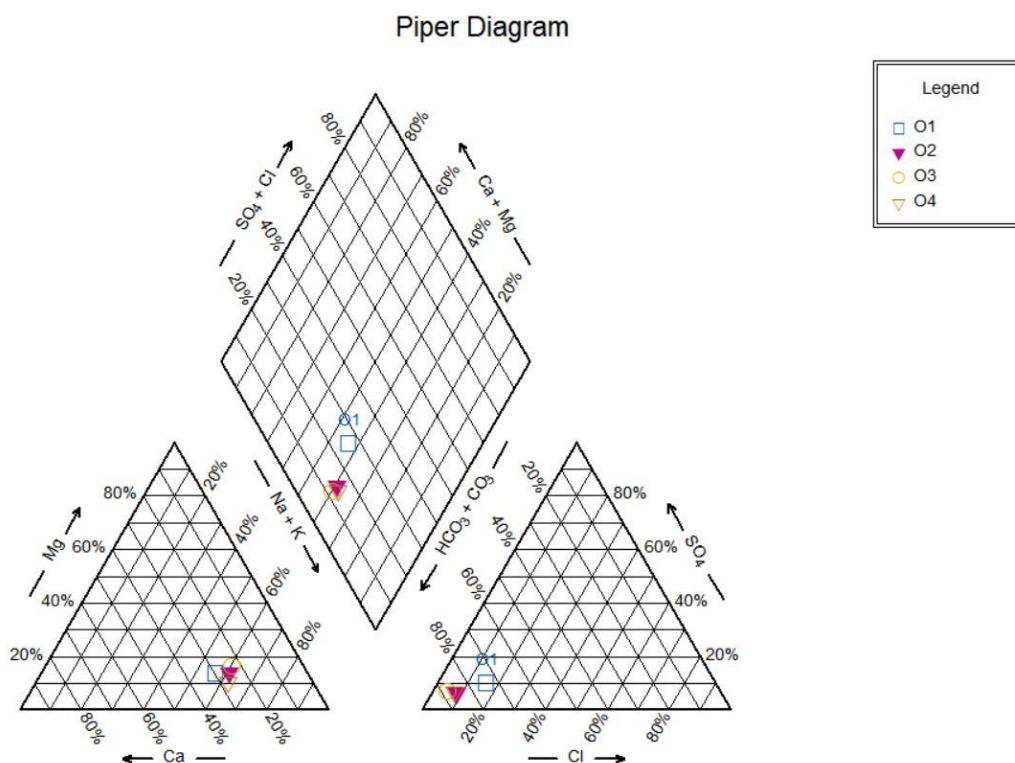


**Figure 1 Piper three-line diagram of Water Samples in Ordovician Limestone Aquifer**

## (2) Sandstone fissure aquifer above 5 coal (V)

The aquifer is located in the upper boundary of the Damiaozhuang Formation 5 coal and Tangjiazhuang Formation of the Lower Permian. The average thickness of this layer is 100m. Lithology is mainly siltstone and sandstone, and sandstone cements are mostly calcium, silica and argillaceous. The rock fissures in this formation are well developed and mainly inclined fissures. It belongs to fractured aquifer with weak water-rich characteristic. The aquifer can be divided into lower part (V<sub>A</sub>) and upper part (V<sub>B</sub>):

The lower part (V<sub>A</sub>): This part is located at 0 - 60 m above 5 coal. It is fluvial facies sandstone and has scouring contact with underlying strata. In the western and central part of the minefield, coal strata are scoured directly to coal 5 or 6, or even to coal 7 or 8. The unit water inflow in this part is 0.05-0.092 L/s·m. The permeability coefficient is 2.552 m/d. It is a fractured aquifer with weak water-rich.

The upper part ( $V_B$ ): This part is located at 60 - 100 m above 5 coal. The roof of this part is directly connected with the weathering zone of bedrock. The unit water inflow in this section is 0.087 L/s·m. The permeability coefficient is 1.722 - 2.059 m/d. It is fractured aquifer with weak water-rich.

This aquifer is exposed in the second level roadway of the mine. The maximum water inflow is 9.9 m<sup>3</sup>/min during construction, and then decreases gradually. At present, the second level of mining has basically ended, so this aquifer does not affect the mining activities in this mining area. The hydrochemical characteristics Piper three-line diagram of the representative water samples of this aquifer are shown in Figure 2.

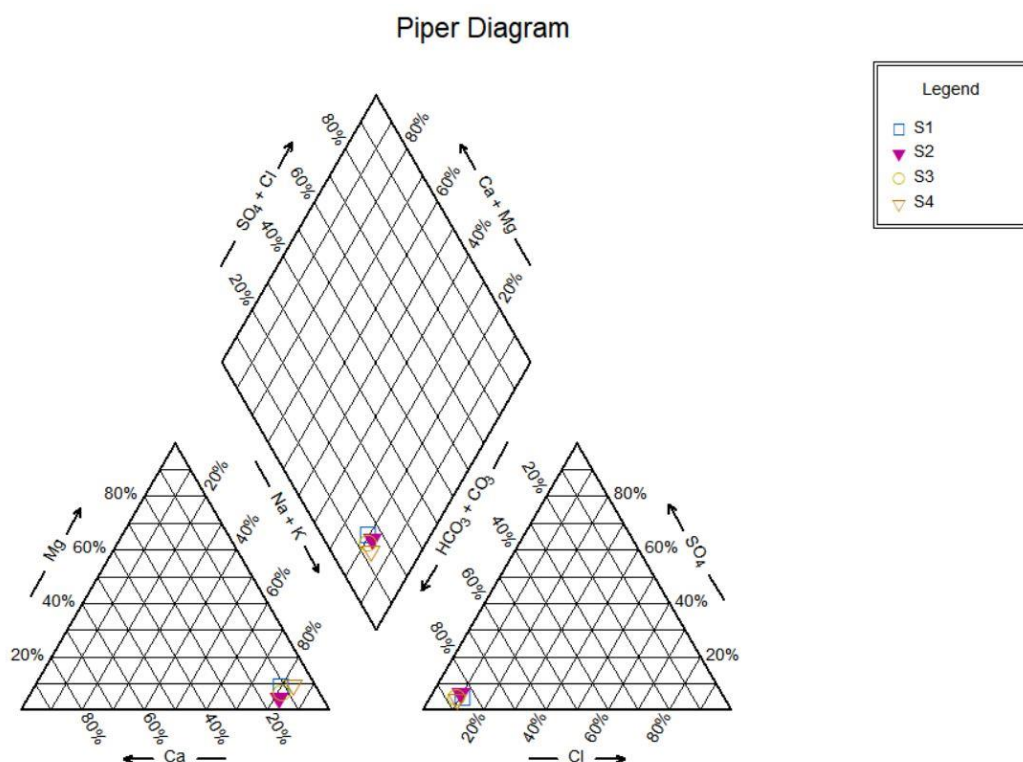


**Figure 2 Piper three-line diagram of Water Samples in sandstone fissure aquifer**

### (3) Sand-gravel pore aquifer in the upper Quaternary (VIII)

The thickness of the aquifer is 100 - 379.67m. It is composed of unequal grains of gravel, pebble and clay. Among them, 80% are coarse sand and gravel, 10% are pebble and 10% are clay. The aquifer is relatively homogeneous, but the amount of clay in the gravel is different, which results in different properties of water-rich. The aquifer is well developed in the southeastern part of the well field. It almost contacts with the bedrock directly to recharge the bedrock aquifers. In the lower part of the northwest part of the

stratum, clay layers directly cover the bedrock. The clay layer has good water resistance. Due to this clay layer, there are two forms of recharge relationship between this aquifer and 5 coal roof sandstone fractured aquifer: skylight type and overflow type. The hydrochemical characteristics Piper three-line diagram of the representative water samples of this aquifer are shown in Figure 3.

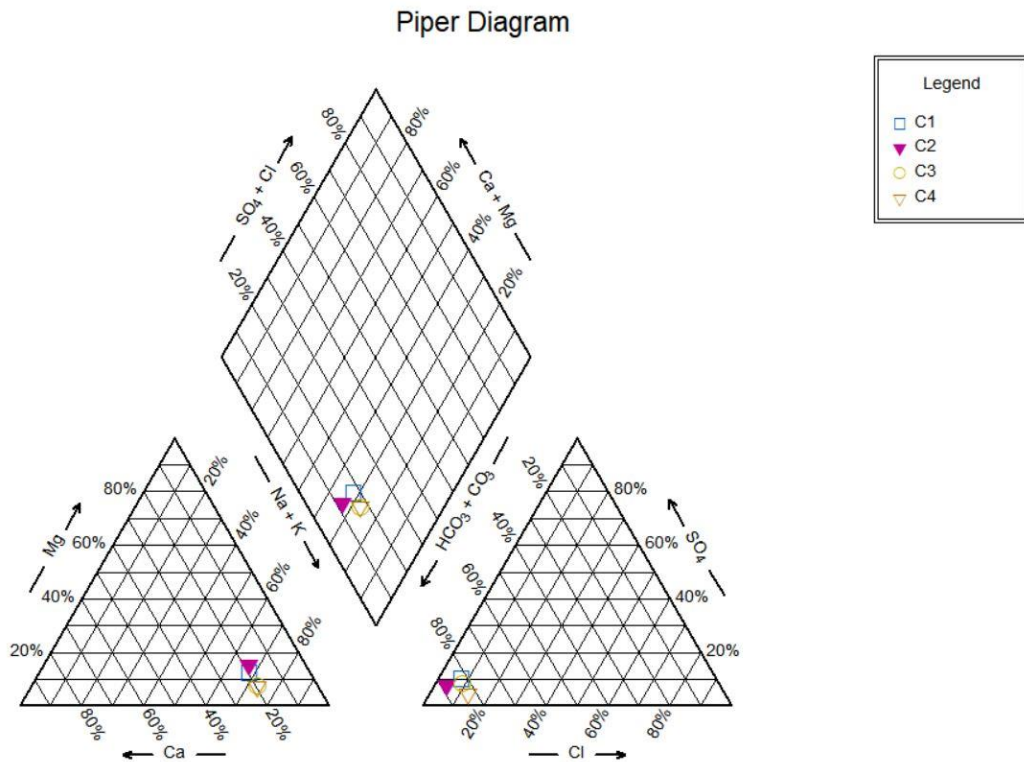


**Figure 3 Piper three-line diagram of Water Samples in Quaternary alluvial aquifer**

### 3.4.2 Hydrochemical Characteristics of Mixed Simulated Water Samples

#### (1) Hydrochemical types

AqQA software was used to analyze the hydrochemical characteristics of water samples mixed in different proportions. The hydrochemical Piper diagram of the original water sample and the mixed water sample was drawn. The changes of hydrochemical types after mixing were analyzed.

After mixing the water samples of the Ordovician limestone karst fissure confined aquifer (I) and Sand-gravel pore aquifer in the upper Quaternary (VIII), the hydrochemical type has not changed. It is still  $\text{HCO}_3\text{-Ca}$  type. Water sample O1 from Ordovician limestone karst fissure confined aquifer (I) and water sample C1 from Sand-

gravel pore aquifer in the upper Quaternary (VIII) mix in different proportions as shown in Figure 4.

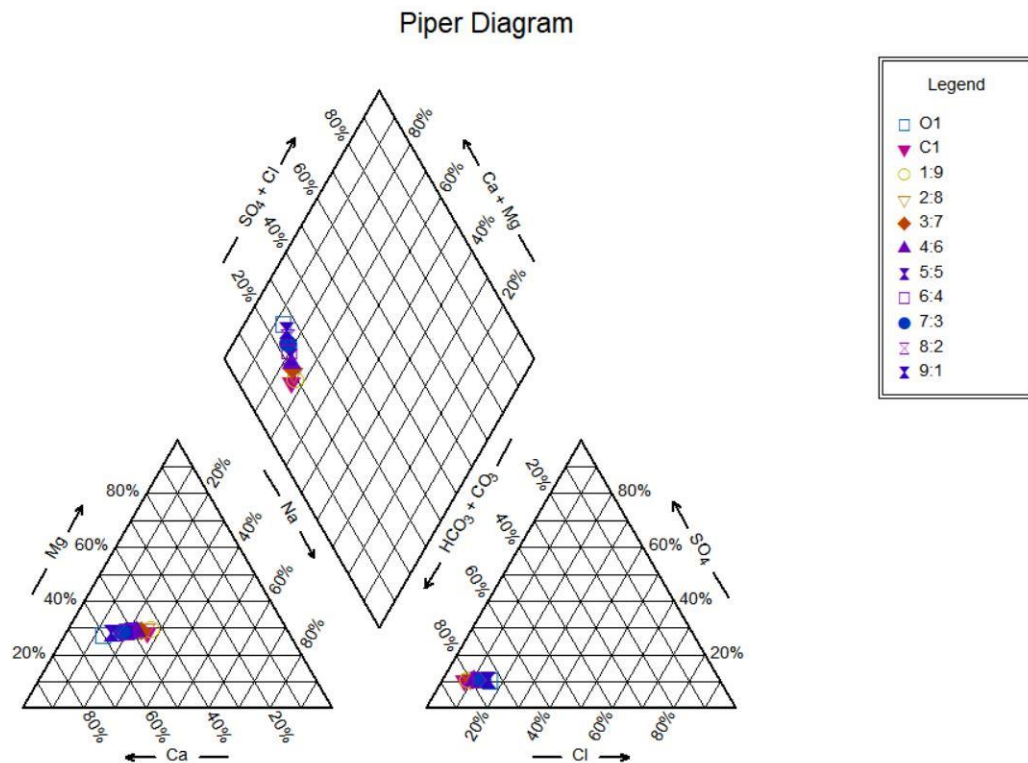


**Figure 4 Piper Diagram of Water Sample O1 and C1 Mixed in Different Proportions**

After mixing the water samples of Ordovician limestone karst fissure confined aquifer (I) and Sandstone fissure aquifer above 5 coal (V), the hydrochemical types of water samples changed from  $\text{HCO}_3\text{-Ca}$  type to  $\text{HCO}_3\text{-Na}$  type.

The mixing results of the water samples O1 from Ordovician limestone karst fissure confined aquifer (I) and the water samples S1 from Sandstone fissure aquifer above 5 coal (V) in different proportions are shown in Figure 5.

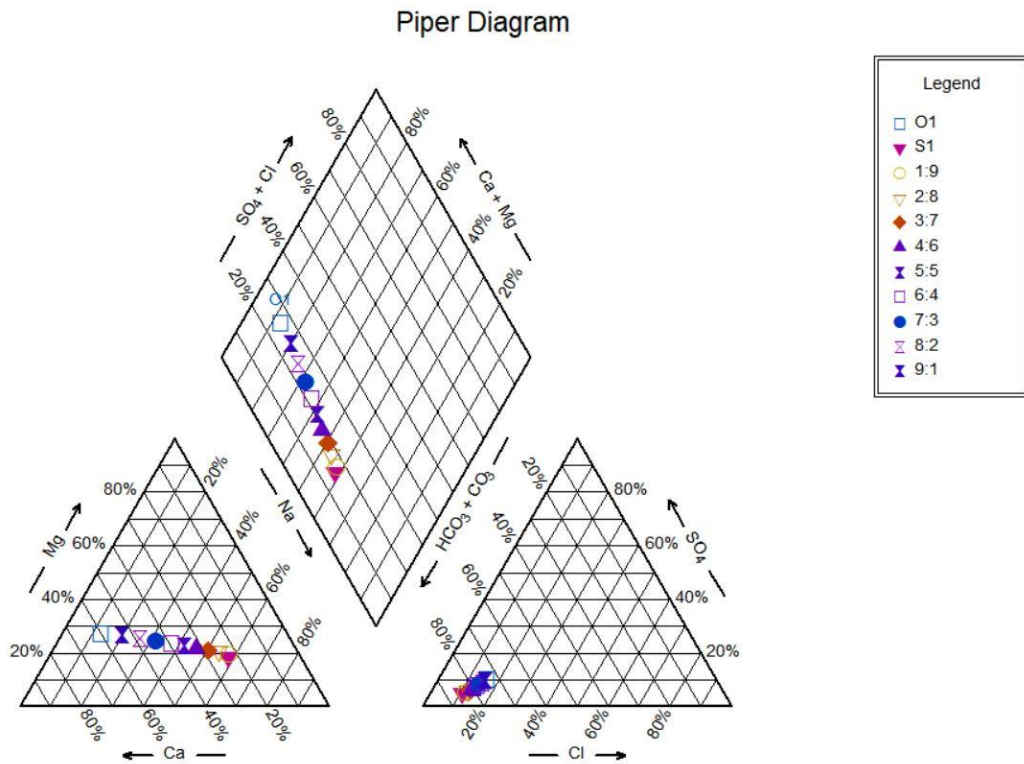


**Figure 5 Piper Diagram of Water Sample O1 and S1 Mixed in Different Proportions**

After mixing the water samples of Sand-gravel pore aquifer in the upper Quaternary (VIII) and Sandstone fissure aquifer above 5 coal (V), the hydrochemical types of water samples changed from  $\text{HCO}_3\text{-Ca}$  type to  $\text{HCO}_3\text{-Na}$  type.

The mixing results of the water samples C1 from Sand-gravel pore aquifer in the upper Quaternary (VIII) and the water samples S1 from Sandstone fissure aquifer above 5 coal (V) in different proportions are shown in Figure 6.

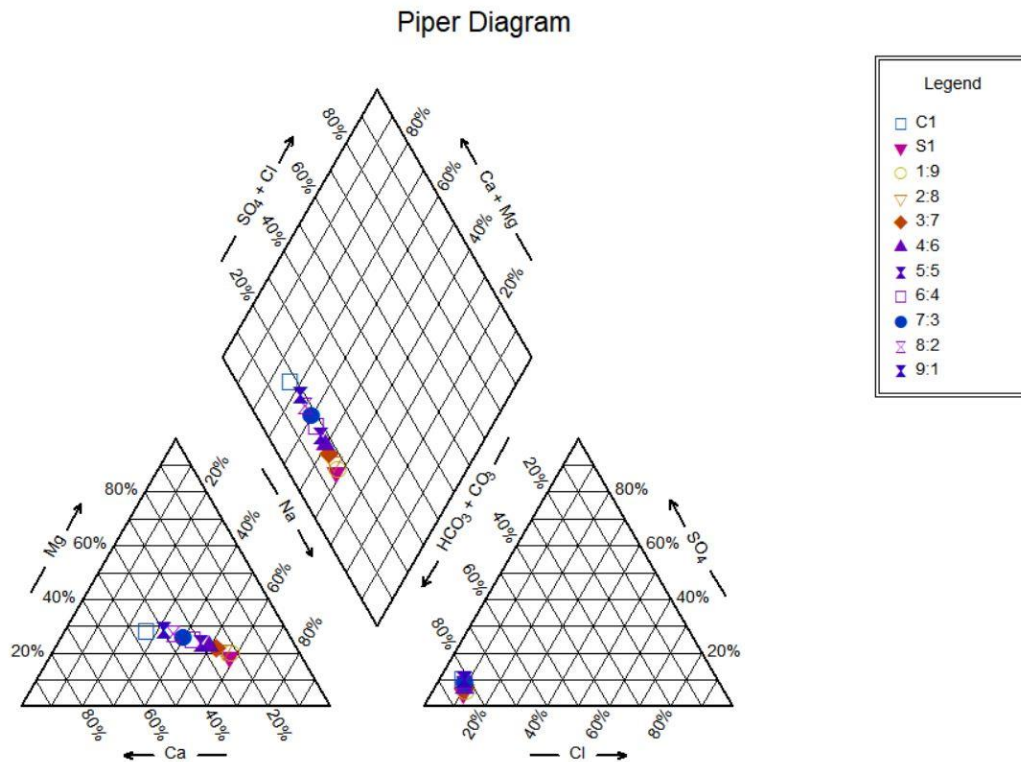


**Figure 6 Piper Diagram of Water Sample C1 and S1 Mixed in Different Proportions**

## (2) Variety of Ion Concentration

Data statistics software Origin was used to analyze the hydrochemical characteristics of raw water samples mixed in different proportions. The line chart of the concentration distribution of conventional ions including the original water sample and the mixed water sample were drawn. The change of conventional ion concentration in aquifers after mixing was analyzed.

Water samples from Ordovician limestone karst fissure confined aquifer (I) and Sand-gravel pore aquifer in the upper Quaternary (VIII) have mixed. With the increase of mixing ratio, the concentration of  $\text{HCO}_3^-$  ions increased the most, followed by  $\text{Na}^+$  ions in solution. The concentration of other ions did not change much.

Water sample O1 from Ordovician limestone karst fissure confined aquifer (I) and water sample C1 from Sand-gravel pore aquifer in the upper Quaternary (VIII) mix in different proportions as shown in Figure 7.

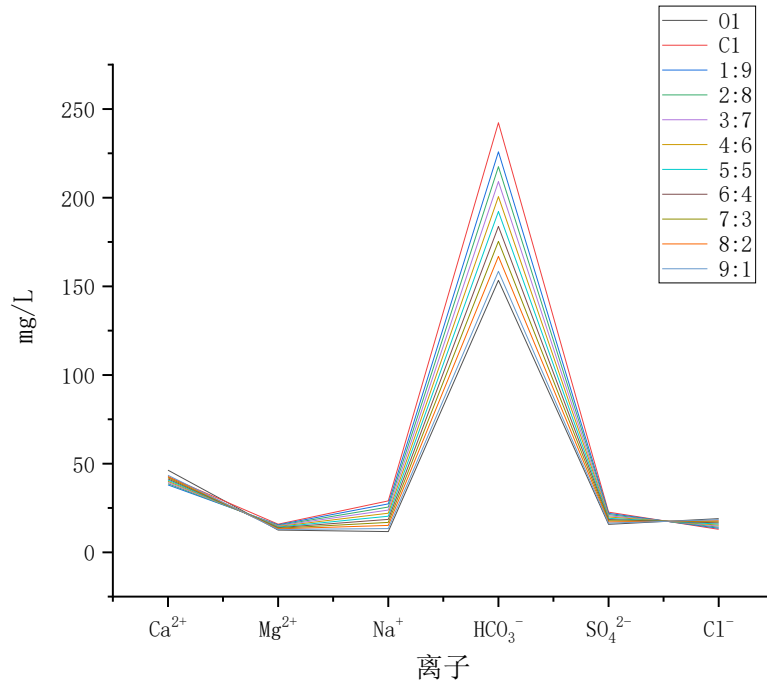


**Figure 7 Line Chart of Water Sample O1 and C1 Mixed in Different Proportions**

Water samples from Ordovician limestone karst fissure confined aquifer (I) and Sandstone fissure aquifer above 5 coal (V) have mixed. With the increase of mixing ratio, the concentration of HCO<sub>3</sub><sup>-</sup> and Na<sup>+</sup> ions changed greatly, which increase range was very large. The second is Ca<sup>2+</sup> ions in solution, which decreases in a certain range. The concentration of other ions did not change much.

The mixing results of the water samples O1 from Ordovician limestone karst fissure confined aquifer ( I ) and the water samples S1 from Sandstone fissure aquifer above 5 coal ( V ) in different proportions are shown in Figure 8.



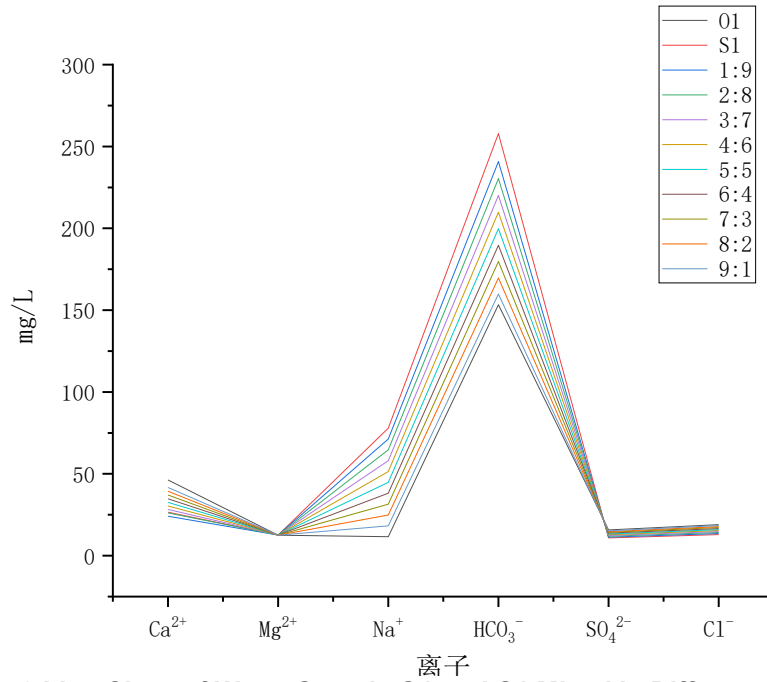


**Figure 8 Line Chart of Water Sample O1 and S1 Mixed in Different Proportions**

Water samples from Sand-gravel pore aquifer in the upper Quaternary (VIII) and Sandstone fissure aquifer above 5 coal (V) have mixed. With the increase of mixing ratio, the concentration of Na<sup>+</sup> ions changed greatly, which increase range was very large. The second is Ca<sup>2+</sup> ions in solution, which decreases in a certain range. The concentration of other ions did not change much.

The mixing results of the water samples C1 from Sand-gravel pore aquifer in the upper Quaternary (VIII) and the water samples S1 from Sandstone fissure aquifer above 5 coal (V) in different proportions are shown in

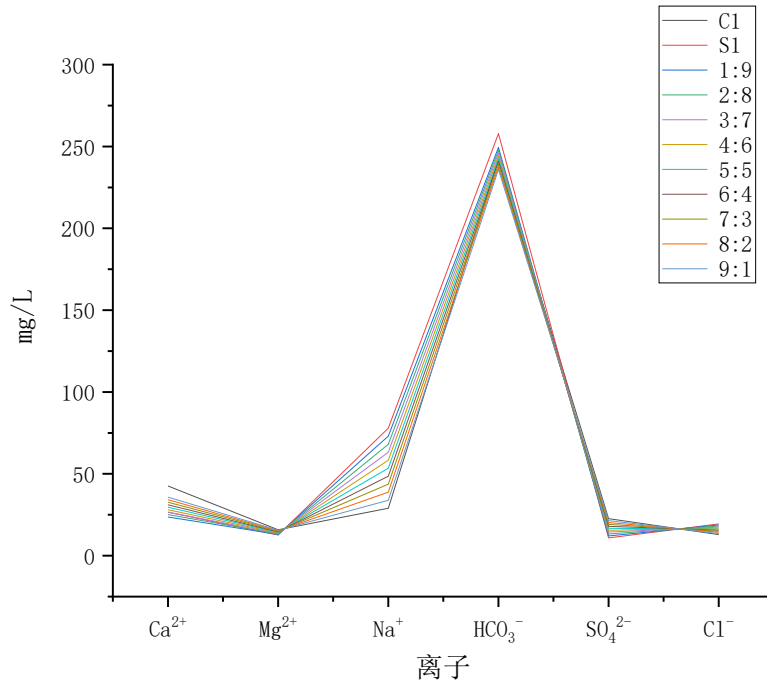


**Figure 9 Line Chart of Water Sample C1 and S1 Mixed in Different Proportions**

---

## **4 Research on Identification Model of Inrush Water Source**

---

There are various ions in groundwater. The composition of groundwater varies greatly under different conditions. When water inrush occurs, the water source is usually not a single aquifer, but a mixture of underground aquifer water sources. This will make us face enormous challenges in identifying the source of water inrush. In this case, uncertain mathematical models emerge as the times require. It can better simulate the uncertainty of groundwater to a certain extent, thus increasing the reliability of discrimination.

In Kailuan mining area, there are differences in the recharge and drainage of aquifers, acidity and alkalinity, which leads to the different types and contents of ion components in groundwater. Through the mixed simulation method described in Chapter 4, a large number of water samples of Jinggezhuang mine aquifer are simulated by PHREEQC. The mixed simulated water sample data are selected and sorted out as the input layer data of the mixed water source discrimination model. The establishment method of artificial neural network hybrid water inrush source identification model is studied, and the accuracy of water source identification is verified, which provides a scientific means for mine water hazard prevention and control.

Artificial neural network has the characteristics of self-organization, self-adaptation and fault-tolerance. It is widely used in system pattern recognition, classification, prediction and so on. The application of artificial neural network (ANN) to mine water inrush source identification will give full play to its unique advantages, which has certain application value and significance (Xu X & Wang G, 2016).

---

### **4.1 Basic Ideas of BP Neural Network**

---

The early development of artificial neural networks (ANNs) was driven by the desire to simulate the learning process of biological systems, including the human brain. Consistency is an important concept in nonparametric estimation. The uniform estimator is an estimator that converges asymptotically to the estimated object (e.g. regression function) under large sample size. When the sample size tends to be infinite, the uniform estimator is a model, which can approximate the objective function with arbitrary precision. In other words, when there is enough data available, there is an

unbiased model. Many researchers at home and abroad have proved that artificial neural network can approximate any function to the desired accuracy.

Therefore, many early studies of artificial neural networks focused on their ability to accurately learn the data sets presented (i.e. training sets). Although the above work tends to focus on function approximation, early research in the field of classification includes the design of neural networks to achieve the goal of complete and correct classification of training sets. In conclusion, these works show that the design of neural networks can generate unbiased estimates for given classification data.

According to the continuity of the value of the neuron, the artificial neural network can be divided into two types: continuous network and discrete network. According to the different network structure, it can also be divided into two categories: namely the Feedback Network and the Feedforward Network. The hierarchical relationship of feedforward network is very clear. The information flow flows from input layer to output layer in one direction (Li D et al., 2015).

BP (Back Propagation) neural network is a multi-layer feedforward network trained by error back propagation algorithm. It was proposed by Rinehart and McClelland in 1986. BP neural network can learn and store a large number of mapping relationships without revealing the mathematical equation of input-output mode mapping relationship in advance. The steepest descent method is used to adjust the weights and thresholds of the network through back propagation, and finally iterate to minimize the sum of squares of errors of the network.

It is necessary to adjust the weights of the network through repeated and continuous cycles in order to make it more reasonable. Therefore, in order to obtain the allowable error range, we need to debug repeatedly when constructing the neural network (Qi R, 2018). The structure sketch of BP neural network is shown in Figure 10.

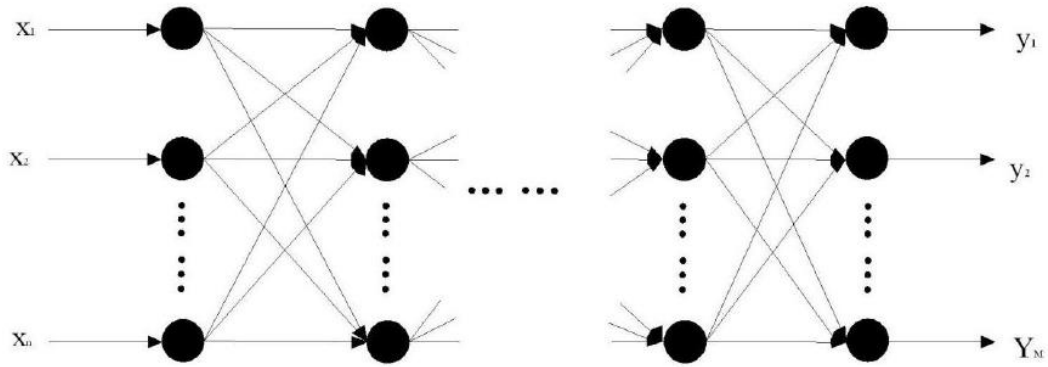


Figure 10 The schematic diagram of BP neural network structure

BP neural network mainly relies on the back propagation of the output layer error to the hidden layer to get the expected value of the output layer.

In order to make the output error as small as possible, the gradient descent method is used to calculate and adjust the weight of the neural network. The expression of error function is as follows:

$$E = \frac{1}{2} \sum (T_k - O_k)^2$$

$T_k$  is and are target values, and  $O_k$  is output values.

The gradient descent method affects the weight by changing the gradient error:

$$\Delta W_{ij} = -\eta \times \frac{\partial E}{\partial W_{ij}}$$

$\eta$  is learning efficiency.  $\frac{\partial E}{\partial W_{ij}}$  is expressed in the following formula:

$$\frac{\partial E}{\partial W_{ij}} = -\delta_j^n \cdot A_i^{n-1}$$

The gradient error can be obtained as follows:

$$\Delta W_{ij} = \eta \cdot \delta_j^n \cdot A_i^{n-1}$$

The connection weight  $W_{ij}$  will affect the output layer result  $A_i^{n-1}$ . The error signal is represented by  $\delta_j^n$ , which is related to the connection weight  $W_{ij}$ . After a series of calculations,  $\delta_j^n$  can quickly identify whether  $j$  is a neuron in the output layer. If so, the following formula holds:

$$\delta_j = (T_j - Y_j) \cdot Y_j \cdot (1 - Y_j)$$

If  $j$  is a neuron in the hidden layer, the following formula holds:

$$\delta_j = \left| \sum_i \delta_i \cdot (W - hy)_{hj} \right| \cdot H_h \cdot (1 - H_h)$$

$H_h$  is the value of the hidden layer. The weight equation is as follows:

$$W_{ij}^m = W_{ij}^{m-1} + \Delta W_{ij}^m = W_{ij}^{m-1} + \eta \cdot \delta_j^n \cdot A_i^{n-1}$$

In fact, the error signal is equivalent to the expected output minus the actual output value. The weight of the network is dynamically adjusted in the process of error back propagation, which reduces the network discrimination error gradually (Lee, 2008; LiouHuang & Yang, 2008; Jiang S, Sun Y, Yang L, & Ling C, 2007).

---

## 4.2 Establishment of BP Neural Network Model for Recognition of Water Inrush Source

---

In order to create a neural network for identifying water inrush sources, sample data should be selected first. In the study area, aquifer water samples which may be the source of water inrush are collected. The main data are hydrochemical characteristics, including pH, concentration indicators of  $\text{Ca}^{2+}$ ,  $\text{Mg}^{2+}$ ,  $\text{K}^+\text{+Na}^+$ ,  $\text{HCO}_3^-$ ,  $\text{Cl}^-$ ,  $\text{SO}_4^{2-}$ . A certain number of representative water samples are selected in each aquifer as raw water sample data. Using the hydrochemical simulation software PHREEQC, the original representative water samples of different aquifers are simulated by the method mentioned in Chapter 4. Mixing proportions can be selected from small to large (e.g. 1:9, 2:8, 3:7, 4:6, 5:5, 6:4, 7:3, 8:2, 9:1). The water sample data after mixed simulation is used as the data set of the neural network model.

Based on TensorFlow software, about 85% of the mixed water samples in this data set are selected as training samples of the neural network, and the remaining 15% of the water samples are used as validation samples.  $\text{Ca}^{2+}$ ,  $\text{Mg}^{2+}$ ,  $\text{K}^+\text{+Na}^+$ ,  $\text{HCO}_3^-$ ,  $\text{Cl}^-$ ,  $\text{SO}_4^{2-}$ , and pH were taken as seven hydrochemical characteristics of water samples. An initial BP neural network is established based on TensorFlow.

The algorithm of establishing a BP neural network discriminant model based on TensorFlow software includes the following steps: Firstly, the data are standardized and normalized to values between 0 and 1. Next, the input neurons are input to

establish the input layer. The error is calculated by the error loss function, and the cross-entropy loss function is selected.

Thirdly, gradient descent method is used to optimize the discriminant model, and ADAM Optimizer is used as the optimize algorithm. Finally, the treated water sample data are trained and tested. The number of iterations is 5000 - 10000, which ensures the accuracy of the neural network discriminant model.

---

#### 4.2.1 Data Preprocessing Method

---

When using TensorFlow software to build a BP neural network discriminant model, the data should be pre-processed first. Scaling data to a small specific interval is called normalization of data. Converting data into dimensionless pure values can not only eliminate the influence and limitation of units on data, but also facilitate the comparison and weighting of data in different units or scales. The most typical one is mapping data to [0,1] interval.

Min-max standardization is the most commonly used method of data normalization. Min-max standardization, also known as 0-1 standardization, is a linear transformation of data, so that the transformed data range falls into the [0,1] interval. The conversion function is as follows:

$$x^* = \frac{x - \min}{\max - \min}$$

Max is the maximum value of sample data and min is the minimum value of sample data. The code used is:

```
def Normalization(x):
```

```
    return [(float(i)-min(x))/float(max(x)-min(x)) for i in x]
```

---

#### 4.2.2 Error Loss Function

---

When the neural network model of water inrush source identification is established, the cross-entropy loss is chosen as the error loss function.

Cross-entropy loss is a common loss function in classification tasks. Although many researchers have used the square error cost function in practice, the cross-entropy loss function has several theoretical advantages. Firstly, the square error assumes the

Gauss target data, which is contrary to the given binary target training neural network classifier. On the other hand, the measurement based on entropy is specially developed for binary objectives. This may significantly affect the effectiveness of neural network prediction. Secondly, the square error can be controlled by outliers at some points with very large errors. Cross-entropy has little influence on logarithmic linear error function. Thirdly, the square error function depends on the square of absolute error. At the same time, the cross-entropy error depends on the relative error of network output. Therefore, cross-entropy may perform better in both large and small target values, because they often lead to similar relative errors. This shows that the cross-entropy function performs better than the square error function in estimating the small posteriori probability(Kline & Berardi, 2005).

The connotation of cross-entropy refers to the difference between the actual output and the expected output. That is to say, the smaller the value of cross-entropy is, the closer the distribution of expected output is to that of actual output. If the expected output probability distribution is  $p(x)$ , the actual output probability distribution is  $q(x)$ , and the cross-entropy is  $H(p, q)$ , then:

$$H(p, q) = - \sum_x p(x) \log q(x)$$

In BP neural network, the activation function is needed to convert multiple linear inputs into non-linear relations. Because the expression ability of linear model is often insufficient in the face of the actual application, the activation function can introduce non-linear factors. Otherwise each layer of neural network only does simple linear transformation, and the multi-layer input superposition is still linear transformation, which can not meet the actual needs.

When using TensorFlow to establish the identification model of Water Inrush Source Based on neural network, two hidden layers of neural network are selected., the Sigmoid activation function is recommended for the selection of cross-entropy loss function in the process of data transfer between the input layer and the first hidden layer, and between the first and the second hidden layer.

The expression of Sigmoid activation function is as follows:

$$\sigma(z) = \frac{1}{1 + e^{-z}}$$



The image of function  $\sigma(z)$  is shown in Figure 11 Cross-Entropy Simoid Activation Function Curve.

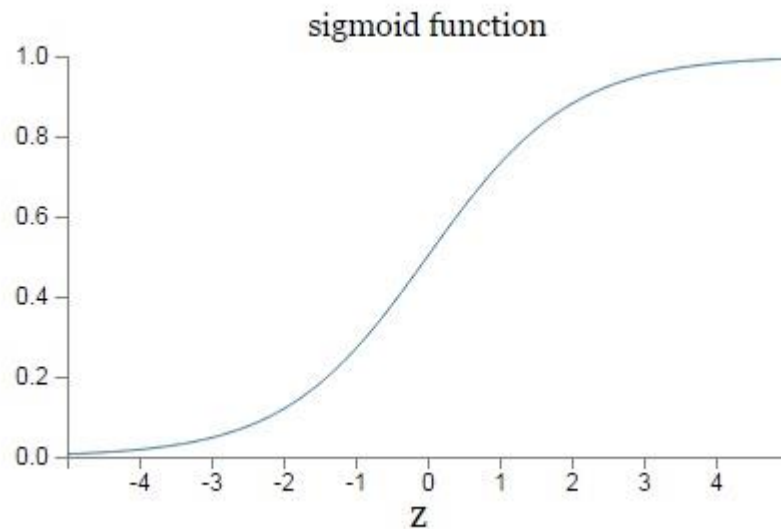


**Figure 11 Cross-Entropy Simoid Activation Function Curve**

The use of cross-entropy loss function and Sigmoid activation function will ensure that the neural network model keeps a high gradient state when it converges. The function characteristics of Sigmoid itself lead to the problem that the convergence speed of the model is very slow when the training results are close to the real value. Because the cross-entropy loss function is a logarithmic function, it can remain in a high gradient state when it approaches the upper boundary. The slope of the upper boundary and the lower boundary decreases very quickly, which can improve the problem.

When data transfer between the second hidden layer and the output layer, the Softmax activation function is selected for the Softmax regression.

It's supposed that the original output of the neural network is  $y_1, y_2, \dots, y_n$ , then the output after the Softmax regression processing is as follows:

$$\text{softmax}(y_i) = y'_i = \frac{e^{y_i}}{\sum_{j=1}^n e^{y_j}}$$

The output mode is changed from a single node to a probability value.

---

### 4.2.3 Model Optimization by Gradient Descent Method

---

When the neural network model of water inrush source identification is established, the gradient descent method is used to optimize the model to minimize the error function. ADAM algorithm is used as the optimizing algorithm.

In order to improve the convergence of this gradient descent method, it is a common method to introduce the adaptive step size. The adaptive step size is a numerical process for solving continuous problems, which is a step discretization process.

ADAM optimization algorithm is one of the most popular gradient descent optimization algorithms. It is implemented in common neural network frameworks, such as TensorFlow, Caffe or CNTK. Kingma and BA prove that the Adam optimizer is faster than any other optimizer through experiments (see Figure 12 Comparison of different optimizer by training of multilayer). Ruder, Sebastian (Ruder, 2017) said: "ADAM is the first multi-layer neural network to be trained on MNSIT images so far, which may be the best overall choice compared with different optimizers." All these points show the importance of neural network optimization program and the superiority of ADAM optimizer.

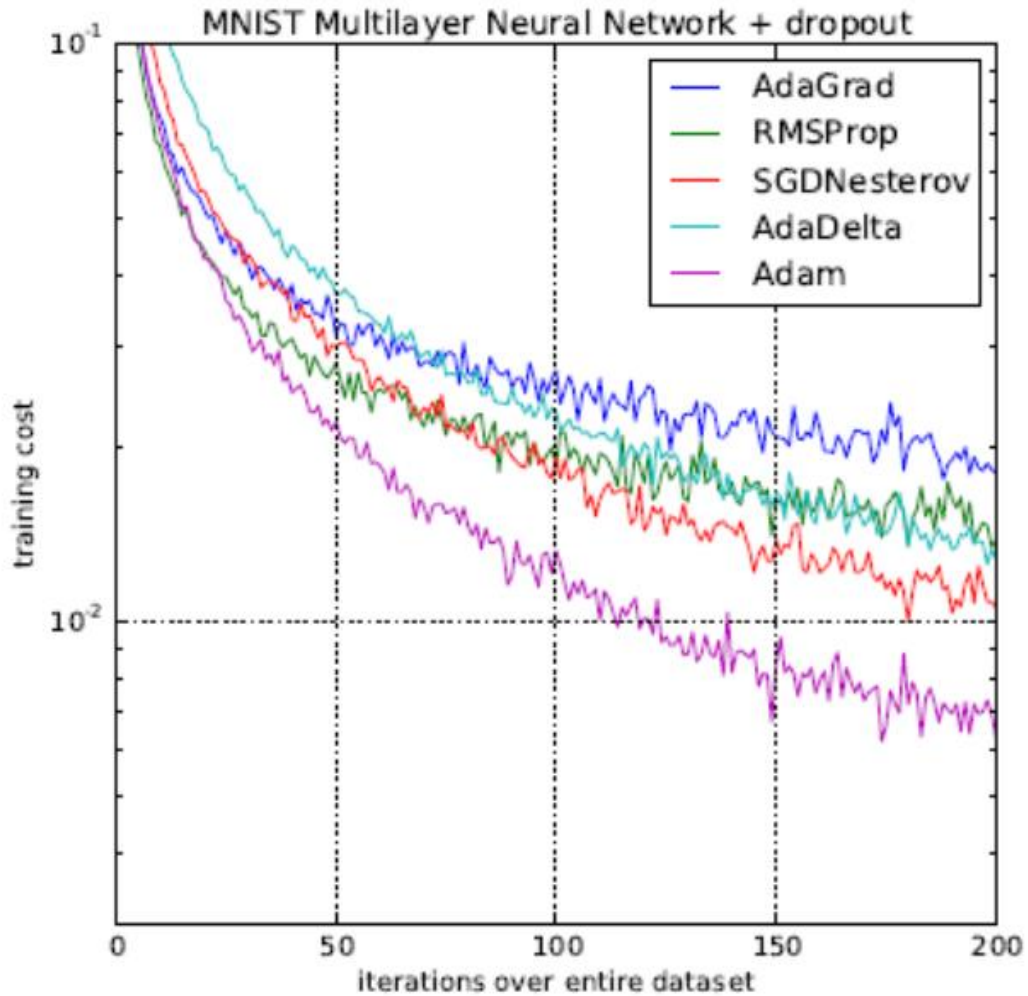


**Figure 12 Comparison of different optimizer by training of multilayer neural networks on MNIST images**

(1) Method of Moments

Moment method is based on adaptive step size. First, we define our weight change rules.

Definition 1 (Weight Change Rule)

Let  $w \in R^n$  be the weight vector of the neural network,  $e(w)$  be the error function, and  $\eta \in R^+$  be the step size. In addition, let  $t \in N$  be the timestamp of the current training step. Then  $w(t)$  is the weight vector in the training step  $t$ .

$$w(t + 1) = w(t) + \Delta w(t)$$

$$\Delta w(t) = -\frac{\eta}{2} \nabla_w e(w(t))$$

When using the rules in the definition, the errors of the neural network can be minimized by increasing the weight. The shape of  $\nabla w(t)$  depends on the method chosen. The moments method adds a part of weight to the gradient descent step, which changes from the previous timestamps.

#### Definition 2 (Method of Moments)

Let  $\alpha \in R^+$  be the decay rate of the old weight change. All other parameters are defined according to Definition 1. Weight change will be defined as follows:

$$\Delta w(t) = -\frac{\eta}{2} \nabla_w e(w(t)) + \alpha \Delta w(t-1)$$

In order to attain convergence of the method of moments, the restriction  $\alpha \in [0, 1]$  should be applied.

#### (2) ADAM-Optimizer

The adaptive moment estimation (ADAM) was invented by Kingma and Ba and is nowadays one of the most popular step size methods in the area of neural networks. The algorithm is defined as follows.

**Data:**  $\eta_t = \frac{\eta}{\sqrt{t}}$  as step size,  $\beta_1, \beta_2 \in (0, 1)$  as decay rates for the moment estimates,  $\beta_{1,t} := \beta_1 \lambda^{t-1}$  with  $\lambda \in (0, 1)$ ,  $\epsilon > 0$ ,  $e(w(t))$  as the initial weight vector.

Set  $m_0 = 0$  as initial 1<sup>st</sup> moment vector

Set  $v_0 = 0$  as initial 2<sup>nd</sup> moment vector

Set  $t = 0$  as initial time stamp

**while**  $w(t)$  not converged **do**

$t = t + 1$

$g_t = \nabla_w e(w(t))$

$m_t = \beta_{1,t} m_{t-1} + (1 - \beta_{1,t}) g_t$

$v_t = \beta_2 v_{t-1} + (1 - \beta_2) g_t^2$

$\hat{m}_t = \frac{m_t}{1 - \beta_1^t}$

$\hat{v}_t = \frac{v_t}{1 - \beta_2^t}$

$$w(t) = w(t - 1) - \eta_t \frac{\hat{m}_t}{(\sqrt{\hat{v}_t} + \epsilon)}$$

**end**

**return** w(t)

Their experiments show that the convergence speed of Adam optimizer is much faster than that of other optimizers for multi-layer or convolutional neural networks.

---

### 4.3 Verification of Water Inrush Source Identification in Jinggezhuang Mine

---

According to the method of building neural network water source identification model mentioned above, the mixed water source identification model of Jinggezhuang Mine is established to verify the feasibility of this method. The data source of the model is the water sample of underground aquifer in Jinggezhuang mining area which is mixed by PHREEQC hydrochemical simulation software according the method mentioned in Chapter 4. The water samples of different aquifers are mixed in different proportions as the classification basis.

Taking the three aquifers of Ordovician limestone karst fissure confined aquifer (I), sandstone fissure aquifer above coal 5 (V) and sand-gravel pore aquifer in upper Quaternary (VIII) as representative aquifers, the mixing ratio can be 2:8, 4:6, 6:4 and 8:2. There are 12 categories totally. The classification can be found in Table 6 Water Source Classification Table of Mixed Water Source Identification Model.

<b>Catogary number</b>	<b>Inrush water souce</b>	<b>Mixing ratio</b>
1	Ordovician limestone water I and sandstone fissure water V	2:8
2	Ordovician limestone water I and sandstone fissure water V	4:6
3	Ordovician limestone water I and sandstone fissure water V	6:4
4	Ordovician limestone water I and sandstone fissure water V	8:2
5	Ordovician limestone water I and quaternary water VIII	2:8
6	Ordovician limestone water I and quaternary water VIII	4:6
7	Ordovician limestone water I and quaternary water VIII	6:4
8	Ordovician limestone water I and quaternary water VIII	8:2
9	Sandstone fissure water V and quaternary water VIII	2:8

10	Sandstone fissure water V and quaternary water VIII	4:6
11	Sandstone fissure water V and quaternary water VIII	6:4
12	Sandstone fissure water V and quaternary water VIII	8:2

**Table 6 Water Source Classification Table of Mixed Water Source Identification Model**

There are 12 neurons in the output layer. Each neuron is a 12-dimensional vector, which is  $(1,0,0,\dots,0)$ ,  $(0,1,0,\dots,0)$ ,  $\dots$ ,  $(0,0,\dots,0,1,0)$  and  $(0,0,\dots,0,0,1)$ , corresponding to each water source category.

128 mixed water samples were selected for each category of inrush water source from mixed simulation water samples by PHREEQC. A total of 1536 water samples were collected from 12 categories of water inrush sources, which contribute to the discriminant model database. 200 water samples were selected as test data, and remaining 1336 water samples were used as training data. The pH, concentration of  $\text{Ca}^{2+}$ ,  $\text{Mg}^{2+}$ ,  $\text{K}^{+}+\text{Na}^{+}$ ,  $\text{HCO}^{-}$ ,  $\text{Cl}^{-}$ ,  $\text{SO}_4^{2-}$  ions were taken as seven hydrochemical characteristics of water samples.

Firstly, the min-max method is used to preprocess the data and standardize it. With the help of TensorFlow library function, an initial BP neural network with seven inputs (corresponding to seven hydrochemical characteristics) and 12 outputs (corresponding to 12 types of water sources) containing two hidden layers is established.

The number of neurons in the input layer is [7], the number of neurons from the input layer to the first hidden layer is [7,14], the number of neurons from the first hidden layer to the second hidden layer is [14,10], and the number of neurons from the second hidden layer to the output layer is [10,12]. Then set the placeholder of water type and category, as well as the weights and biases of each layer. Activation function is used to connect all layers of network. The transfer function of the first and second hidden layer is 'Sigmoid', and the transfer function of the output layer is 'Softmax'.

```
hidden_opt1 = tf.matmul (X, W1) + B1
```

```
hidden_opt1 = tf.nn.sigmoid (hidden_opt1)
```

```
hidden_opt2 = tf.matmul (hidden_opt1, W2) + B2
```

```
hidden_opt2 = tf.nn.sigmoid (hidden_opt2)
```

```
hidden_opt3 = tf.matmul (hidden_opt2, W3) + B3
```

```
hidden_opt3 = tf.nn.softmax (hidden_opt3)
```

The parameters set of the neural network are shown in Table 7 Parameter Setting Table of Neural Network.

Attributes	Set value	Default value
Training steps	10000	100
Interval parameters for displaying	100	25
Training target error	0.05	0
Nodes of first layer	14	7
Nodes of second layer	10	7

**Table 7 Parameter Setting Table of Neural Network**

The initial loss value and the correct rate of loss function are calculated in the model. The ADAM-Optimizer algorithm in gradient descent method is used to optimize the model and minimize the error function. Iterative training and testing are followed, and the loss and accuracy of each step are recorded. Iterative training and test functions:

```

for i in range(lr) :
    #batch = xy_data.train.next_batch (batch_size)
    batch_input = xy_data_train[:test,:7]
    batch_labels = xy_data_train[:test,7:]
    training_loss = sess.run (opt, feed_dict = {X: batch_input, Y: batch_labels})
    record_loss[i] = sess.run(loss, feed_dict={X: batch_input, Y: batch_labels})
    accuracy_data[i] = sess.run(accuracy, feed_dict={X: batch_input, Y:
batch_labels})
    test_accuracy[i] = sess.run(accuracy,feed_dict={X : xy_data_test[:,7:], Y:
xy_data_test[:,7:]})
    if i % 1000 == 0 :
        train_accuracy = accuracy.eval (session = sess, feed_dict = {X: batch_input,Y:
batch_labels})
        print ("step : %d, training accuracy = %g " % (i, train_accuracy))

```

After 10,000 iterations, the final model error of the neural network is small. The error loss of the neural network is shown in Figure 13 Error Loss Curve of Neural Network Model during Iteration. After training of 1336 mixed water sample data, the accuracy of

training results is high, approaching 90%. See Figure 14 Training Accuracy Curve of Neural Network Model.

After testing 200 mixed water samples, the test accuracy can also meet the requirements, which is more than 80%. See Figure 15 Test Accuracy Curve of Neural Network Model. The discriminant accuracy of TensorFlow-based neural network hybrid water source discriminant model can meet the demands, which can provide guidance for actual mine water inrush identification.

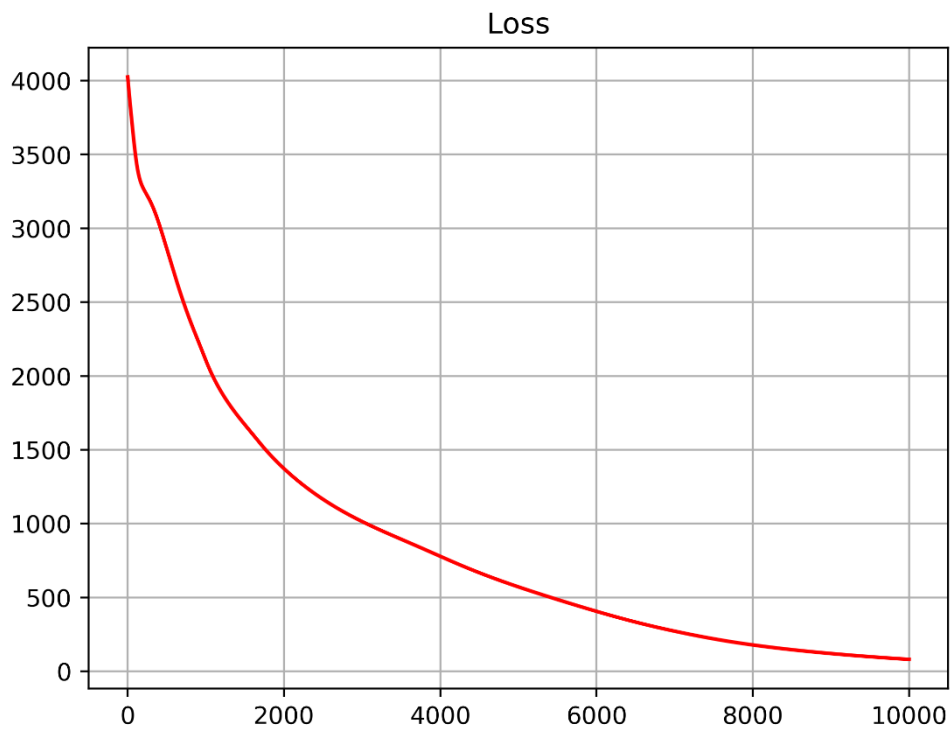


**Figure 13 Error Loss Curve of Neural Network Model during Iteration**



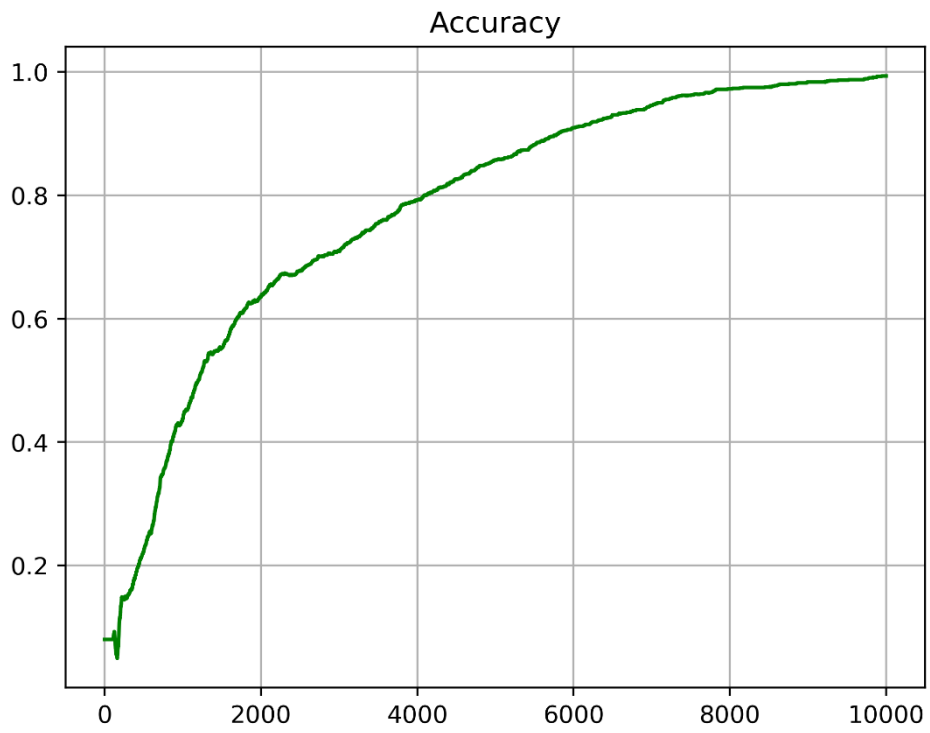


**Figure 14 Training Accuracy Curve of Neural Network Model**

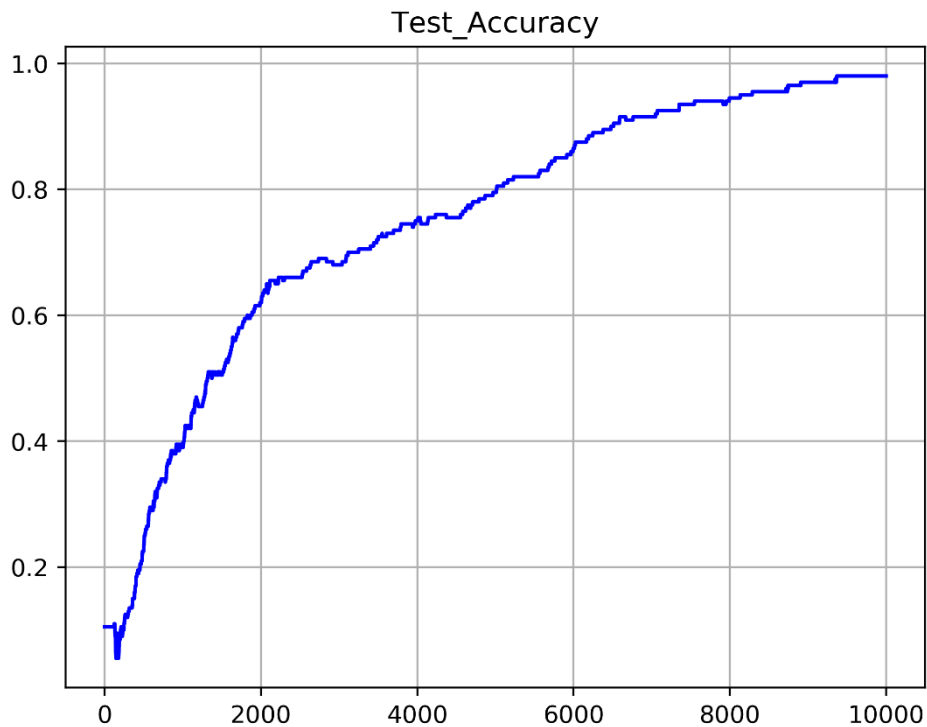


**Figure 15 Test Accuracy Curve of Neural Network Model**

#### 4.4 Error Analysis

The training accuracy of Jinggezhuang Neural Network Mixed Water Source Discrimination Model is almost 90%, and the testing accuracy is over 80%, which can be improved in the future. There may be two reasons for the miscarriage of justice:

(1) Quantity of mixed water sample data

There are 12 categories of water sources and 1536 mixed water samples in the model, which means there are 128 samples for each category. Compared with the number of water source categories, the quantity of data in each category is slightly insufficient. If the number of samples of each category of water source can be increased In the future practical application of this discriminant model, the training and testing accuracy will be further improved. The discriminant accuracy will be also improved accordingly.

(2) Differences between different categories of data

In this research model, each category data of water source is simulated from mixing different aquifers in different proportions. Therefore, there is not enough difference

between different categories of water samples data, which results in slight similarity between different categories. To a certain extent, this affects the accuracy of the neural network identification model and increases the probability of misjudgment. If the requirement of mixing proportion identification is not so accurate like Jinggezhuang in actual application of mining area, the accuracy of identifying inrush water source will further increase.

---

## 5 Conclusions and Innovation

---

### 5.1 Main Research Conclusions

---

Taking Jinggezhuang Mine in Kailuan Mining Area as the object of analysis, this paper collected and collated the water quality data obtained from many years' observation in the mining area. Mixing simulation of water sample data was carried out by PHREEQC hydrochemical simulation software, and its hydrochemical characteristics were analyzed. The establishment method of identification mixed inrush water source in mining area is studied. The following conclusions are drawn:

(1) The water quality types of aquifers in Kailuan Jinggezhuang mining area are analyzed by Piper Diagram. The hydrochemical characteristics of groundwater in Jinggezhuang Mine are generally characterized by high concentration of  $\text{Ca}^{2+}$ ,  $\text{K}^{+}+\text{Na}^{+}$ ,  $\text{HCO}_3^-$ . The hydrochemical types of Ordovician limestone karst fissure confined aquifer (I) and sand-gravel pore aquifer in upper Quaternary (VIII) are mainly  $\text{HCO}_3\text{-Ca}$  type, and those of sandstone fissure aquifer above coal 5 (V) are mainly  $\text{HCO}_3\text{-Na}$  type.

(2) The mix of groundwater samples were simulated hydrochemically by PHREEQC software in Jinggezhuang mining area. The hydrochemical types of mixed water samples changed between  $\text{HCO}_3\text{-Ca}$  and  $\text{HCO}_3\text{-Na}$ , and the ion concentration also changed greatly. The main ions that changed were  $\text{Ca}^{2+}$ ,  $\text{K}^{+}+\text{Na}^{+}$ ,  $\text{HCO}_3^-$ , which were anions and cations with higher ion concentration in water samples.

(3) A TensorFlow-based artificial neural network mixed water source identification model is proposed. After data pre-processing and data standardization, cross-entropy error loss function and excitation function are used to reduce errors. Then, ADAM Optimizer is used to optimize the identification model. Finally, the data of water samples are trained and tested iteratively for several times to ensure that training accuracy of the neural network identification model is almost 90%, and that the identification accuracy of the neural network identification model for mixed water inrush sources reaches more than 80%.

---

### 5.2 Innovations

---

The extraction method of mixing ratio of Water Inrush Source in Kailuan mining area was established. With PHREEQC hydrochemical simulation software, mixing of Identification and Simulation Study of Mixing Inrush Water Source

groundwater samples was simulated in Jinggezhuang mining area, and the hydrochemical characteristics of mixed water samples of aquifers were studied, which is of innovative significance for the study of the hydrochemical characteristics of the mixed water source of mine water inrush in Kailuan Mining Area.

Based on the water sample data after hydrochemical mixing simulation, a method of establishing the identification model of hybrid water source based on TensorFlow artificial neural network was proposed. This paper completed the discriminant study on the source and proportion of mixed water inrush in mine, and provides a new way to discriminate the source of mixed water inrush in mine area.

---

## 6 Bibliography

---

1. Bhat NA, Jeelani GH: Delineation of the recharge areas and distinguishing the sources of karst springs in Bringi watershed, Kashmir Himalayas using hydrochemistry and environmental isotopes. *Journal of Earth System Science* 124:1667-1676, 2015.
2. Clark ID, Fritz P: *Environmental Isotopes in Hydrogeology* Lewis, 1997.
3. Davis A, Ashenberg D: The aqueous geochemistry of the Berkeley Pit, Butte, Montana, U.S.A. *Applied Geochemistry* 4:23-36, 1989.
4. Epstein S, Mayeda T: Variation of O 18 content of waters from natural sources. *Geochimica Et Cosmochimica Acta* 4:213-224, 1953.
5. Gammons CH, Poulson SR, Pellicori DA, et al.: The hydrogen and oxygen isotopic composition of precipitation, evaporated mine water, and river water in Montana, USA. *Journal of Hydrology* 328:319-330, 2006.
6. Kline DM, Berardi VL: Revisiting squared-error and cross-entropy functions for training neural network classifiers. *Neural Computing & Applications* 14:310-318, 2005.
7. Lee TL: Back-propagation neural network for the prediction of the short-term storm surge in Taichung harbor, Taiwan. *Engineering Applications of Artificial Intelligence* 21:63-72, 2008.
8. Li P, Hui Q, Wu J, et al.: Química de iones mayoritarios en el agua subterránea superficial en Dongsheng Coalfield, Ordos Basin, China. *Mine Water & the Environment*, 2013.
9. Liou CY, Huang JC, Yang WC: Modeling word perception using the Elman network. *Neurocomputing* 71:3150-3157, 2008.
10. Meng Y, Liu G: Isotopic characteristics of precipitation, groundwater, and stream water in an alpine region in southwest China. *Environmental Earth Sciences* 75:894, 2016.
11. Merkel BJ: *Principles and Applications of Groundwater Geochemical Modeling*: China University of Geosciences Press, 2005.
12. Montety VD, Marc V, Emblanch C, et al.: Identifying the origin of groundwater and flow processes in complex landslides affecting black marls: Insights from a hydrochemical survey. *Earth Surface Processes & Landforms* 32:32-48, 2010.
13. O'Shea B, Jankowski J: Detecting subtle hydrochemical anomalies with multivariate statistics: an example from 'homogeneous' groundwaters in the Great Artesian Basin, Australia. *Hydrological Processes* 20:4317-4333, 2010.
14. Ruder S: *An overview of gradient descent optimization algorithms.*, 2017.
15. Wang R, Bian JM, Gao Y: Research on hydrochemical spatio-temporal characteristics of groundwater quality of different aquifer systems in Songhua River Basin, eastern Songnen Plain, Northeast China. *Arabian Journal of Geosciences* 7:5081-5092, 2014.

16. Yidana SM, Banoeng B: Analysis of groundwater quality using multivariate and spatial analyses in the Keta basin, Ghana. *Journal of African Earth Sciences* 58:220-234, 2010.
17. Yue W, Wang N, Zhao L, et al.: Hydrochemical characteristics and recharge sources of Lake Nuoertu in the Badain Jaran Desert. *Chinese Science Bulletin* 59:886-895, 2014.
18. Chen C, Wang J, Dong S, et al.: Discrimination model of Water Inrush Source in Jiaozuo mining area. *Coalfield geology and exploration*: 38-40, 1996.
19. Chen L: *Hydrogeochemical Characteristics of Groundwater in Northern Anhui Mining Area*, 2003.
20. Chen L, Gui H, Hu Y, et al.: Isotope discriminant model for karst water environment of coal seam floor in northern Anhui mining area. *Coal science and technology*: 44-47, 2003.
21. Chen L.: *Hydrogeochemical Evolution and Identification of Groundwater in Mining Areas*: Beijing: Geological Publishing House, 2007.
22. Cheng C, Ge X, Wang D: Hydrogeochemical Characteristics of Baishan Mining Area and Their Application in Discrimination of the Source of Mine Outflow Water. *Journal of Huainan Institute of Mining Technology*: 25-32, 1994.
23. Fan J, Li H, Xie F, et al.: Application of Fuzzy Probability Method in Identifying Water Inrush Sources in Mines. *Zhongzhou Coal*: 1-2, 2000.
24. Gao W, He Y, Li X: Application of hydrochemical method in judging water source of mine water inrush. *Mining safety and environmental protection*: 44-45, 2001.
25. Ge Z, Shen W, Bai H: A preliminary study on hydrogeology of mine water inrush from an Ordovician limestone aquifer in Xuzhou Coal Mine. *Jiangsu Geology*: 91-96, 1994.
26. Gui H, Xu G, Song X: Water-filling Conditions and Water Source Identification of Taoyuan Coal Mine. *Journal of Huainan Vocational and Technical College*: 85-86, 2003.
27. Gui H, Chen L, Peng Z: Principal Component Analysis of Trace Elements in Deep Karst Water in Northern Anhui Mining Area. *Coalfield Geology and Exploration*: 31-34, 2004.
28. Gui H, Chen L, Song X: Using tritium content to study the characteristics of deep groundwater circulation in northern Anhui mining area. *Geological frontier*: 351-352, 2004.
29. Gui H, Chen L: Study on the Mixing Model of Environmental Isotopes in Deep Groundwater in Northern Anhui Mining Area. *Coal Science and Technology*: 68-71, 2005.
30. Jiang C, Zhang S: Coal mine water inrush prediction model based on neural network. *Journal of Heilongjiang University of Science and Technology*: 8-11, 2006.
31. Jiang S, Sun Y, Yang L, et al.: Prediction of mine water inflow based on BP neural network method. *Coalfield geology of China*: 38-40, 2007.
32. Jin Z: *Study on Comprehensive Discrimination Model of Water Inrush Source in Xinji No. 1 Mine*, Anhui University of Technology, 2016.

33. Lei X, Zhang J and Xie T: Prediction of coal mine water inrush based on genetic neural network. *Computer Engineering*: 132-133, 2003.
34. Li D: Prediction and evaluation of coal mine water inrush by using neural network. *Coal*: 18-19, 1998.
35. Li D, Zhou K, Sun W, et al.: Application analysis of BP neural network and SVM in mine environmental assessment. *Arid region geography* 38:128-134, 2015.
36. Li D: Hydrochemical characteristics of main aquifers and identification of water inrush sources in Baimiao Coal Mine. *Karst in China*: 295-304, 1995.
37. Li M: Application of Fuzzy Similarity Ratio in Discrimination of Mine Water Inrush Source. *Coal Engineer*: 28-31, 1995.
38. Li M, Yu Y, Lu F, et al.: Fuzzy Comprehensive Evaluation Model of Water Inrush Source in Yaoqiao Coal Mine. *Survey Science and Technology*: 16-20, 2001.
39. Liu F: Hydrogeochemical Exploration Technology for Mine Water Sources. *Coalfield Geology and Exploration*: 62-64, 2007.
40. Liu J, Chang J, Hun B: Research and Application of Integrated Water Control Technology in Kailuan Mining Area. *Shaanxi Coal*: 62-63, 2008.
41. Liu X: Using hydrochemical characteristics to distinguish water source of mine gushing (outburst). *Xu Coal Science and Technology*: 15-16, 1999.
42. Qi R: Analysis of hydrochemical characteristics of Panbei mine in Huainan and identification model of water inrush source. *Anhui University of Technology*, 2018.
43. Song X, Gui H, Chen L: Geochemical characteristics of trace elements in the main aquifers of northern Anhui mining area. *China Coal*: 38-40, 2004.
44. Song X, Gui H, Chen L: Bayesian multiclass linear discriminant analysis of trace elements in groundwater of Huaibei coalfield. *China Coal*: 42-44, 2005.
45. Sun B, Duan Z, Jin H: Automatic identification of water source discrimination model in Renlou Coal Mine. *Coalfield geology and exploration*: 44-48, 1999.
46. Sun Z, Gao W: Water source analysis of water inrush in 3112 working face of Dongzhuang Coal Mine. *Jiangsu Coal*: 47-49, 1995.
47. Wang G, Duan Q, Bu C, et al.: Some applications of hydrogeochemical methods in the study of water hazards in coal mines - Taking Pingdingshan and Feicheng mining areas as examples. *Geological commentary*: 653-657, 2001.
48. Wang L: Study on Groundwater Chemical Environment in Guyuan Rock Salt Mine, South Ningxia. *China University of Geosciences (Beijing)*, 2012.
49. Wei Y, Liang H, Ren Y, et al.: Application of Neural Network in Discrimination of Water Inrush Sources from Coal Mines. *Jiangsu Geology*: 36-38, 2004.
50. Wu Y: Hydrochemical characteristics of karst water and identification of water inrush sources in Linhuan mining area. *Anhui University of Technology*, 2018.
51. Xia X, Zhang H, Yang W: Determining the water inrush source of Caozhuang Coal Mine by the method of fuzzy comprehensive evaluation. *Western prospecting project*: 54-56, 2002.
52. Xu X, Wang G: Application of BP neural network in identifying mine water inrush source. *Coal technology* 35:144-146, 2016.



53. Yang B, Wang C, Yan C: Cause Analysis of Water Inrush Disaster in Qidong Coal Mine. *Coalfield Geology and Exploration*: 41-43, 2003.
54. Yang J, Wang X, Li S, et al.: Analysis of hydrochemical characteristics of Water Inrush Source in Xin'an mine. *Mining research and development*: 70-73, 2005.
55. Yang Z: Research on Shock Ground Pressure Behavior and Prevention in Kailuan Mining Area. China University of Mining and Technology (Beijing), 2011.
56. Zhang D: Study on hydrochemical characteristics and water source discrimination model of Huainan mining area. Anhui University of Technology, 2017.
57. Zhang P: Study on hydrochemical characteristics and water-rock interaction of the Alshan Spring Group. China University of Geosciences (Beijing), 2017.
58. Zhang R: Analysis of Groundwater Environmental Characteristics and Discrimination Model of Water Inrush Source in Panyi Coal Mine Based on GIS. Hefei University of Technology, 2008.
59. Zhang X, Zhang Z and Peng S: Application of Quantitative Theory in the Discrimination of Water Source of Mine Outburst (Gushing). *Journal of China University of Mining and Technology*: 42-45, 2003.
60. Zhang Y, Jiang Z: Discrimination Model and System Realization of Water Source Type of Mine Water Inrush. *Coalfield Geology and Exploration*: 35-37, 2003.
61. Zhou L, Li X: Grey system theory is applied to analyze the super-large water inrush in No. II(617) working face of Yangzhuang Mine. *Journal of Huainan Institute of Mining and Technology*: 8-13, 1995

---

## 7 List of Figures

---

Figure 1 Piper three-line diagram of Water Samples in Ordovician Limestone Aquifer .....	28
Figure 2 Piper three-line diagram of Water Samples in sandstone fissure aquifer ....	29
Figure 3 Piper three-line diagram of Water Samples in Quaternary alluvial aquifer ..	30
Figure 4 Piper Diagram of Water Sample O1 and C1 Mixed in Different Proportions	31
Figure 5 Piper Diagram of Water Sample O1 and S1 Mixed in Different Proportions	32
Figure 6 Piper Diagram of Water Sample C1 and S1 Mixed in Different Proportions	33
Figure 7 Line Chart of Water Sample O1 and C1 Mixed in Different Proportions .....	34
Figure 8 Line Chart of Water Sample O1 and S1 Mixed in Different Proportions .....	35
Figure 9 Line Chart of Water Sample C1 and S1 Mixed in Different Proportions .....	36
Figure 10 The schematic diagram of BP neural network structure .....	39
Figure 11 Cross-Entropy Simoid Activation Function Curve .....	43
Figure 12 Comparison of different optimizer by training of multilayer .....	45
Figure 13 Error Loss Curve of Neural Network Model during Iteration .....	50
Figure 14 Training Accuracy Curve of Neural Network Model .....	51
Figure 15 Test Accuracy Curve of Neural Network Model .....	52

---

## 8 List of Tables

---

Table 1 Hydrochemistry information of the Ordovician limestone aquifer water samples .....	23
Table 2 Hydrochemistry information of the sandstone fissure aquifer water samples	24
Table 3 Hydrochemistry information of the Quaternary alluvial aquifer water samples .....	25
Table 4 Mixed assemblages of representative water samples from each aquifer.....	26
Table 5 Mixing simulation results of water sample O1 and C1 in Jinggezhuang Mine. ....	27
Table 6 Water Source Classification Table of Mixed Water Source Identification Model .....	48
Table 7 Parameter Setting Table of Neural Network .....	49

## Thesis Grade

**Thesis:** Identification and Simulation Study of Mixing Inrush Water Source  
Based on PHREEQC

**Author:** Yixuan Gao

**Supervisor:** Donglin Dong **Grade:** 92 **Signature:** Donglin Dong

**Co-Supervisor:** \_\_\_\_\_ **Grade:** \_\_\_\_\_ **Signature:** \_\_\_\_\_